PA-4.9.2.1 Discretization of Fracture Domain

The fracture domain is discretized in space using the block centered finite difference method indicated in Figure PA-28. In this formulation, cell concentrations are defined at grid block centers while the velocity components $[u, v]$ are defined on grid cell faces. A uniform mesh with 50 m × 50 m cells is used for the spatial discretization. Ghost cells are placed outside the problem domain for the purpose of implementing boundary conditions. The temporal discretization is accomplished using variable time step sizes.

The dispersive term, $\nabla \bullet (\phi D_k \nabla C_k)$, in Equation (223) is approximated using a second-order central difference formula (Fletcher 1988).

The advective term, $\nabla \bullet \mathbf{v} C_k$, is approximated using the Total Variation Diminishing (TVD) method (Sweby 1984). The TVD method provides a way of accurately resolving advection dominated transport problems without the occurrence of nonphysical oscillations commonly present in second-order solutions. This method invokes a weighted upstream differencing scheme that locally adjusts the weighting to prevent oscillatory behavior and maximize solution accuracy. The weighting parameters are known as the TVD flux limiters $\Phi(x, y, r)$, where r is a function of the concentration gradient and direction of flow. PA uses the van Leer TVD limiter (Sweby 1984, p. 1005), which is defined as

$$\Phi(x, y, r) = \max\left\{0, \min\left\{2r, \frac{r + |r|}{1 + |r|}\right\}\right\}. \qquad (240)$$

At locations where u (i.e., the Darcy velocity in the x direction) is positive, r is defined at the j–1/2, k interface by

$$r_{j-1/2,k} = \frac{\partial C/\partial x|_{j-3/2,k}}{\partial C/\partial x|_{j-1/2,k}}, \qquad (241)$$

and at locations where u is negative, r is defined by

$$r_{j-1/2,k} = \frac{\partial C/\partial x|_{j+1/2,k}}{\partial C/\partial x|_{j-1/2,k}}. \qquad (242)$$

Similar definitions are made for r at the j, k–1/2 interface in the y-direction with $\mathbf{v}$ (i.e., the Darcy velocity in the y direction) used instead of u.

Because Φ_k is a function of C_k, the discretized set of equations is nonlinear. This nonlinearity is addressed by treating the flux limiters explicitly (i.e., time lagged). Explicit treatment of the limiter functions, however, can lead to oscillatory and sometimes unstable solutions when the Courant number exceeds unity (Cr > 1), where Cr is defined by

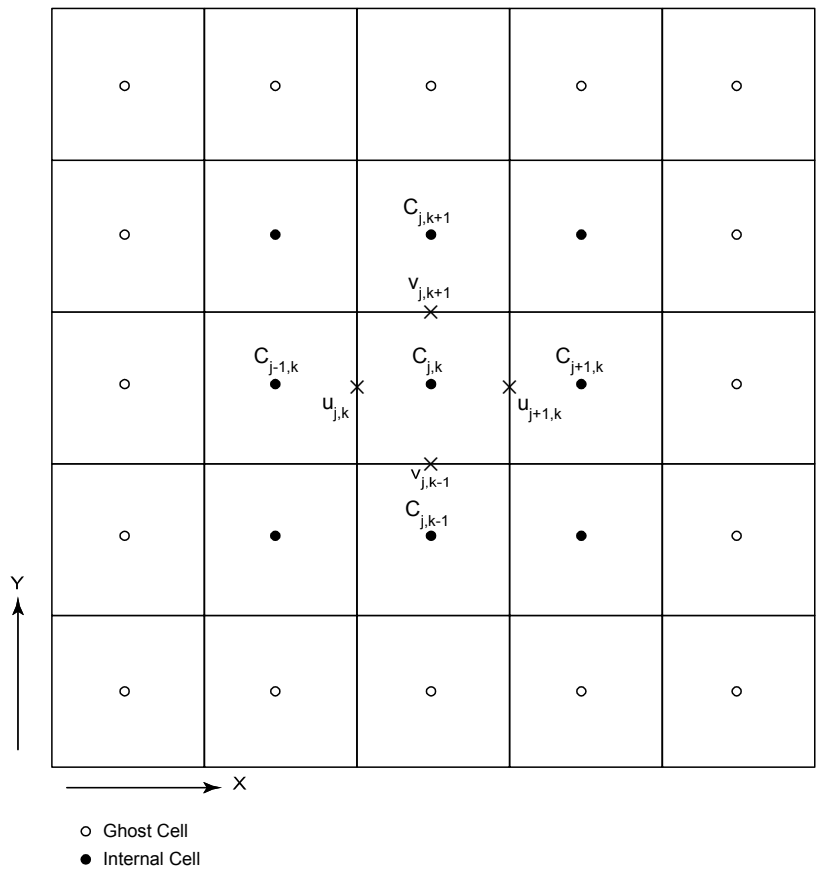

Figure PA-28. Schematic of Finite Volume Staggered Mesh Showing Internal and Ghost Cells.

$$Cr = \max\left\{Cr_x, Cr_y\right\}, \text{ where } Cr_x = |u|\Delta t/\phi\Delta x \text{ and } Cr_y = |v|\Delta t/\phi\Delta y. \qquad (243)$$

To avoid this behavior, the application of the TVD method is restricted to regions in which the Courant numbers are less than one. In regions where Cr > 1, a first order full upwinding scheme is invoked, which is unconditionally stable and nonoscillatory.

The discretized form of Equation (223) can be expressed in a delta formulation as

$$\left(\mathbf{I} + \mathbf{L}_{xx} + \mathbf{L}_{yy} + \mathbf{S}\right)\Delta\mathbf{C}^{n+1} = \mathbf{RHS}^n, \qquad (244)$$

where $\mathbf{I}$ *is the identity matrix,* $\mathbf{L}_{xx}$ *and* $\mathbf{L}_{yy}$ *are finite difference operators in the x and y directions,* $\mathbf{S}$ *is an implicit source term that accounts for decay and mass transfer between the matrix and the fracture,* $\mathbf{RHS}$ *consists of the right hand side known values at time level n, and* $\Delta\mathbf{C}_{n+1} = \mathbf{C}_{n+1} - \mathbf{C}_n$. *Direct inversion of Equation (244) for a typical Culebra transport problem is very computationally intensive, requiring large amounts of memory and time. To reduce these requirements, the operator in Equation (244) is factored as follows:*

$$\left(\boldsymbol{I}+\boldsymbol{L}_{xx}+\alpha_x\boldsymbol{S}\right)\left(\boldsymbol{I}+\boldsymbol{L}_{yy}+\alpha_y\boldsymbol{S}\right)\Delta\boldsymbol{C}^{n+1}=\boldsymbol{RHS}^n, \tag{245}$$

where α_x and α_y are constants that must sum to one (i.e., $\alpha_x + \alpha_y = 1$). The left hand sides in Equation (244) and Equation (245) are not equivalent, with the result that the factorization of Equation (244) in Equation (245) is referred to as an approximate factorization (Fletcher 1988). The advantage of approximately factoring Equation (244) is that the resulting equation consists of the product of two finite difference operators that are easily inverted independently using a tridiagonal solver. Hence, the solution to the original problem is obtained by solving a sequence of problems in the following order:

$$\left(\boldsymbol{I}+\boldsymbol{L}_{xx}+\alpha_x\boldsymbol{S}\right)\Delta\overline{\boldsymbol{C}}=\boldsymbol{RHS}^n, \tag{246}$$

$$\left(\boldsymbol{I}+\boldsymbol{L}_{yy}+\alpha_y\boldsymbol{S}\right)\Delta\boldsymbol{C}^{n+1}=\Delta\overline{\boldsymbol{C}}, \tag{247}$$

$$\boldsymbol{C}^{n+1}=\boldsymbol{C}^n+\Delta\boldsymbol{C}^{n+1}. \tag{248}$$

PA-4.9.2.2 Discretization of Matrix Equation

The nonuniform mesh used to discretize the matrix equation is shown in Figure PA-29. Straightforward application of standard finite difference or finite volume discretizations on nonuniform meshes results in truncation error terms which are proportional to the mesh spacing variation (Hirsch 1988). For nonuniform meshes, the discretization can be performed after a transformation from the Cartesian physical space (χ) to a stretched Cartesian computational space (ξ). The transformation is chosen so that the nonuniform grid spacing in physical space is transformed to a uniform spacing of unit length in computational space (the computational space is thus a one-dimensional domain with a uniform mesh). The transformed equations contain metric coefficients that must be discretized, introducing the mesh size influence into the difference formulas. Then standard unweighted differencing schemes can then be applied to the governing equations in the computational space.

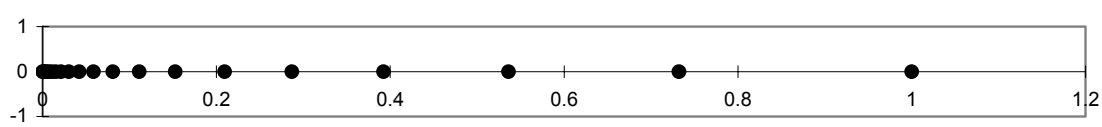

Figure PA-29. Illustration of Stretched Grid Used for Discretization of Matrix Domain.

The SECOTP2D code applies such a coordinate transformation to the nonuniform diffusion domain mesh, solving the transformed system of equations in the uniform computational space. The transformed matrix equation is written as:

$$\phi' R'_k \frac{\partial \hat{C}'_k}{\partial t} - \frac{\partial \hat{F}'_v}{\partial \xi'} = -\phi' R'_k \lambda_k \hat{C}'_k + \phi' R'_{k-1} \lambda_{k-1} \hat{C}'_{k-1}, \tag{249}$$

where

$$\hat{C}'_k = \frac{C'_k}{J}, \tag{250}$$

$$\hat{F}'_v = D'\xi'_x \frac{\partial C'_k}{\partial \xi'}. \tag{251}$$

In the uniform computational space, a first-order backwards difference formula is used to approximate the temporal derivative while a second-order accurate central difference is used to approximate spatial derivatives.

PA-4.9.2.3 Fracture-Matrix Coupling

The equations for the fracture and the matrix are coupled through the mass transfer term Γ_k. In the numerical solution, these equations are coupled in a fully implicit manner and solved simultaneously. A procedure outlined in (Huyakorn et al. 1983) was adapted and redeveloped for an approximate factorization algorithm with the delta formulation and a finite volume grid. The coupling procedure consists of three steps.

Step 1. Write the mass transfer term Γ_k in a delta (Δ) form.

Step 2. Evaluate Δ terms that are added to the implicit part of the fracture equation. This is accomplished using the inversion process (LU factorization) in the solution of the matrix equation. After the construction of the lower tridiagonal matrix L and the intermediate solution, there is enough information to evaluate the Δ terms. This new information is fed into the fracture equation that subsequently is solved for concentrations in the fracture at the new time level (n+1).

Step 3. Construct the boundary condition for the matrix equation at the fracture-matrix interface using fracture concentrations at the (n+1) time level. Matrix concentrations are then obtained using the upper tridiagonal matrix U by back substitution. A detailed description of this technique and its implementation is given in the SECOTP2D User's Manual (WIPP PA 1997b).

PA-4.9.2.4 Cumulative Releases

The cumulative transport $C_k(t,\mathcal{B})$ of individual radionuclides across specified boundaries indicated in Equation (239) is also accumulated during the numerical solution of Equation (223) and Equation (230).

PA-4.9.3 Additional Information

Additional information on SECOTP2D and its use in the CRA-2004 PA to determine radionuclide transport in the Culebra Dolomite can be found in the SECOTP2D User's Manual (WIPP PA 1997b) and in the analysis package for radionuclide transport in the Culebra Dolomite (Kanney 2003).

PA-5.0 PROBABILISTIC CHARACTERIZATION OF SUBJECTIVE UNCERTAINTY

This section summarizes the uncertain parameters in the CRA-2004 PA that constitute the space for subjective uncertainty defined in Section PA-2.4.

PA-5.1 Probability Space

As discussed in Section PA-2.4, the third entity (EN3) that underlies the CRA-2004 PA is a probabilistic characterization of the uncertainty in important variables used as input to the analysis. This entity is defined by a probability space (X_{su}, S_{su}, p_{su}) *that characterizes subjective uncertainty. The individual elements of* S_{su} *are vectors* $\mathbf{x}_{su}$ *of the form*

$$\mathbf{x}_{su} = [x_1, x_2, \ldots x_{nV}], \tag{252}$$

where each x_j *is an imprecisely-known input to the analysis and nV is the number of such inputs.*

The uncertainty in the x_j*, and hence in* $\mathbf{x}_{su}$*, is characterized by developing a distribution*

$$D_j, \; j = 1, 2, \ldots, nV, \tag{253}$$

for each x_j*. Each distribution is based on all available knowledge about the corresponding variable and describes a degree of belief as to where the appropriate value to use for this variable is located. This degree of belief is conditional on the numerical, spatial, and temporal resolution of the models selected for use in the CRA-2004 PA (Chapter PA-4.0). When appropriate, correlations between imprecisely-known variables are also possible, with such correlations indicating a dependency in the knowledge about the correlated variables. It is the distributions in Equation (253) and any associated correlations between the* x_j *that define* (X_{su}, S_{su}, p_{su}).

The uncertain variables (i.e., x_j*) incorporated into the CRA-2004 PA are discussed in Section PA-5.2. Then, the distributions and correlations assigned to these variables are described in Section PA-5.3 and Section PA-5.4. Finally, a discussion of the concept of a scenario is given in Section PA-5.5.*

PA-5.2 Variables Included For Subjective Uncertainty

The CRA-2004 PA selected nV = 64 imprecisely-known variables for inclusion in the analysis (Table PA-17). The individual variables in Table PA-17 correspond to the elements x_j *of the vector* $\mathbf{x}_{su}$ *in Equation (252). Most variables listed in Table PA-17 were also treated as uncertain in the CCA PA (CCA Appendix PAR). Table PA-18 lists the differences between the set of subjectively uncertain variables in the CCA PA and the CRA-2004 PA. Most differences result from the inclusion of additional uncertain variables from the 1997 PAVT. All subjectively uncertain variables incorporated into the CRA-2004 PA are used as input to the models discussed in Section PA-2.3 and Chapter 4.0.*

PA-5.3 Variable Distributions

Each uncertain variable is assigned a distribution that characterizes the subjective uncertainty in that variable. Distributions for each parameter are described in Attachment PAR. Attachment PAR contains documentation for each of the 64 parameters that were sampled by the LHS code during the PA.

PA-5.4 Correlations

Most of the variables in Table PA-17 are assumed to be uncorrelated. However, the pairs (ANHCOMP, ANHPRM), (HALCOMP, HALPRM), and (BPCOMP, BPPRM) are assumed to have rank correlations of –0.99, –0.99, and –0.75, respectively (Figure PA-30, Figure PA-31, and Figure PA-32). These correlations result form a belief that the underlying physics implies that a large value for one variable in a pair should be associated with a small value for the other variable in the pair. The scatterplots in Figure PA-29, Figure PA-30, and Figure PA-31 result from the LHSs described in Section PA-6.4, with the rank correlations within the pairs (ANHCOMP, ANHPRM), (HALCOMP, HALPRM), and (BPCOMP, BPPRM) induced with the Iman and Conover (1982) restricted pairing technique.

The distributions and associated correlations indicated in Table PA-17 and Figure PA-29, Figure PA-30, and Figure PA-31 define the probability space (X_{su}, S_{su}, p_{su}) *for subjective uncertainty in Section PA.2.4. The vector* $\mathbf{x}_{su}$ *in Equation (252) has the form*

$$\mathbf{x}_{su} = [ANHBCEXP, ANHBCVGP, ..., WTAUFAIL], \qquad (254)$$

where the individual elements of $\mathbf{x}_{su}$ *are the subjectively uncertain variables described in Table PA-17.*

PA-5.5 Separation of Stochastic and Subjective Uncertainty

The CRA-2004 PA uses the term "scenario" to refer to subsets E_{st} *of the sample space,* S_{st} *for stochastic uncertainty, with scenario probabilities* $p_{st}(E_{st})$ *being defined by the function* p_{st} *associated with the probability space* (X_{st}, S_{st}, p_{st}) *(Section PA-3.9). This definition is consistent with the concept that a scenario is something that could happen in the future. Subsets* E_{su} *of the sample space for subjective uncertainty* S_{su} *are not referred to as scenarios to maintain the important distinction between the two sample spaces. In particular, a scenario* E_{st} *contains vectors* $\mathbf{x}_{st}$ *of the form defined in Equation (3), and the probability* $p_{st}(E_{st})$ *for* E_{st} *characterizes the likelihood that a vector* $\mathbf{x}_{st}$ *in* E_{st} *will match the occurrences that will take place at the WIPP over the next 10,000 years. In contrast, a subset* E_{su} *from the space of subjective uncertainty* X_{su} *contains vectors* $\mathbf{x}_{su}$ *of the form defined in Equation (252) and the probability* $p_{su}(E_{su})$ *characterizes a degree of belief that a vector* $\mathbf{x}_{su}$ *in* E_{su} *contains the appropriate values for the 64 uncertain variables in Table PA-17.*

Table PA-17. Variables Representing Subjective Uncertainty in the CRA-2004 PA

Sample Position	Variable Name	Material Name	Property Name	Description
1	WGRCOR	STEEL	CORRMCO2	Rate of anoxic steel corrosion (m/s) under brine inundated conditions and with no CO_2 present. Defines R_{ci} in Equation (59) for areas Waste Panel, South RoR, and North RoR in Figure PA-8.
2	WMICDFLG	WAS_AREA	PROBDEG	Index for model of microbial degradation of CPR materials (dimensionless). Used in areas Waste Panel, South RoR, and North RoR in Figure PA-8.
3	WGRMICI	WAS_AREA	GRATMICI	Rate of CPR biodegradation (mol $C_6H_{10}O_5$ / kg $C_6H_{10}O_5$ / s) under anaerobic, brine-inundated conditions. Defines R_{mi} in Equation (61) for areas Waste Panel, South RoR, and North RoR, in Figure PA-8.
4	WGRMICH	WAS_AREA	GRATMICH	Rate of CPR biodegradation (mol $C_6H_{10}O_5$ / kg $C_6H_{10}O_5$ / s) under anaerobic, humid conditions. Defines R_{mh} in Equation (61) for areas Waste Panel, South RoR, and North RoR, in Figure PA-8.
5	WFBETCEL	CELLULS	FBETA	Scale factor used in definition of stoichiometric coefficient for microbial gas generation (dimensionless). Defines β in Equation (77) for areas Waste Panel, South RoR, and North RoR, in Figure PA-8.
6	WRGSSAT	WAS_AREA	SAT_RGAS	Residual gas saturation in waste (dimensionless). Defines S_{gr} in Equation (35) for areas Waste Panel, South RoR, and North RoR in Figure PA-8; also used in waste material in Figure PA-20 for calculation of DBR; see Section PA-4.7.
7	WRBRNSAT	WAS_AREA	SAT_RBRN	Residual brine saturation in waste (dimensionless). Defines S_{br} in Equation (34) for areas Waste Panel, South RoR, and North RoR, in Figure PA-8; also used in waste material in Figure PA-20 for calculation of DBR; see Section PA-4.7.
8	WASTWICK	WAS_AREA	SAT_WICK	Increase in brine saturation of waste due to capillary forces (dimensionless). Defines S_{wick} in Equation (78) for areas Waste Panel, South RoR, and North RoR, in Figure PA-8.

Table PA-17. Variables Representing Subjective Uncertainty in the CRA-2004 PA — Continued

Sample Position	Variable Name	Material Name	Property Name	Description
9	DRZPCPRM	DRZ_PCS	PRMX_LOG	Logarithm of intrinsic permeability (m^2) of the DRZ immediately above the panel closure concrete (Section PA-4.2.8.3). Used in region DRZ_PCS in Figure PA-8.
10	CONPRM	CONC_PCS	PRMX_LOG	Logarithm of intrinsic permeability (m^2) for the concrete portion of the panel closure. (Section PA-4.2.8.1). Used in region CONC_PCS in Figure PA-8.
11	WSOLU4C	SOLU4	SOLCIM	Uncertainty factor (dimensionless) for solubility of U in the +IV oxidation state in Castile brine. Defines UF(Castile, +4, U) in Equation (90).
12	WSOLTH4C	SOLTH4	SOLCIM	Uncertainty factor (dimensionless) for solubility of Th in the +IV oxidation state in Castile brine. Defines UF(Castile, +4, Th) in Equation (90).
14	CONGSSAT	CONC_PCS	SAT_RGAS	Residual gas saturation (dimensionless) in panel closure concrete (Section PA-4.2.8.1). Defines S_{gr} in Equation (35) for area CONC_PCS in Figure PA-8.
15	CONBRSAT	CONC_PCS	SAT_RBRN	Residual brine saturation (dimensionless) in panel closure concrete (Section PA-4.2.8.1). Defines S_{br} in Equation (35) for use in region CONC_PCS in Figure PA-8.
16	CONBCEXP	CONC_PCS	PORE_DIS	Brooks-Corey pore distribution parameter (dimensionless) for panel closure concrete (Section PA-4.2.8.1). Defines λ in Equation (32) for region CONC_PCS of Figure PA-8 for use with Brooks-Corey model; defines λ in $m = \lambda/(1+\lambda)$ in Equation (36) for use with van Genuchten-Parker model in region CONC_PCS.
17	HALPOR	S_HALITE	POROSITY	Halite porosity (dimensionless). Defines ϕ_0 in Equation (25g) for region Salado in Figure PA-8.
18	HALPRM	S_HALITE	PRMX_LOG	Logarithm of intrinsic halite permeability (m^2). Used in region Salado in Figure PA-8.
19	HALCOMP	S_HALITE	COMP_RCK	Bulk compressibility of halite (Pa^{-1}). Defines β_{fB} in Equation (31) for region Salado of Figure PA-8.
20	ANHPRM	S_MB139	PRMX_LOG	Logarithm of intrinsic anhydrite permeability (m^2). Used in regions MB 138, Anhydrite AB, and MB 139 in Figure PA-8.
21	ANHCOMP	S_MB139	COMP_RCK	Bulk compressibility of anhydrite (Pa^{-1}). Defines β_{fB} in Equation (31) for regions MB 138, Anhydrite AB and MB 139 in Figure PA-8.

Table PA-17. Variables Representing Subjective Uncertainty in the CRA-2004 PA — Continued

Sample Position	Variable Name	Material Name	Property Name	Description
22	ANHBCVGP	S_MB139	RELP_MOD	Indicator for relative permeability model (dimensionless) for regions MB 138, Anhydrite AB and MB 139 in Figure PA-8. See Table PA-3.
23	ANRBRSAT	S_MB139	SAT_RBRN	Residual brine saturation in anhydrite (dimensionless). Defines S_{br} in Equation (35) for regions MB 138, Anhydrite AB, and MB 139 in Figure PA-8.
24	ANRGSSAT	S_MB139	SAT_RGAS	Residual gas saturation in anhydrite (dimensionless). Defines S_{gr} in Equation (34) for regions MB 138, Anhydrite AB, and MB 139 in Figure PA-8.
25	ANHBCEXP	S_MB139	PORE_DIS	Brooks-Corey pore distribution parameter for anhydrite (dimensionless). Defines λ in Equation (32) for regions MB 138, Anhydrite AB, and MB 139 of Figure PA-8 for use with Brooks-Corey model; defines λ in $m = \lambda/(1+\lambda)$ in Equations (36) for use with van Genuchten-Parker model in the same regions.
26	SALPRES	S_HALITE	PRESSURE	Initial brine pore pressure (Pa) in the Salado halite, applied at an elevation consistent with the intersection of MB 139. Defines $p_{b,ref}$ for Equation (49) for region Salado in Figure PA-8.
27	BPINTPRS	CASTILER	PRESSURE	Initial brine pore pressure in the Castile brine reservoir. Defines $p_b(x, y, -5)$ in Equation (50) for region CASTILER in Figure PA-8.
28	BPPRM	CASTILER	PRMX_LOG	Logarithm of intrinsic permeability (m^2) of the Castile brine reservoir. Used in region CASTILER in Figure PA-8.
29	BPCOMP	CASTILER	COMP_RCK	Bulk compressibility (Pa^{-1}) of Castile brine reservoir. Defines β_{fB} in Equation (29) for region CASTILER of Figure PA-8
30	BHPERM	BH_SAND	PRMX_LOG	Logarithm of intrinsic permeability (m^2) of the silty sand-filled borehole (Table PA-5). Used in regions Upper Borehole and Lower Borehole in Figure PA-8.
31	DRZPRM	DRZ_1	PRMX_LOG	Logarithm of intrinsic permeability (m^2) of the DRZ. Used in regions Upper DRZ and Lower DRZ in Figure PA-8.
32	PLGPRM	CONC_PLG	PRMX_LOG	Logarithm of intrinsic permeability (m^2) of the concrete borehole plugs (Table PA-5). Used in region Borehole Plugs in Figure PA-8.

Table PA-17. Variables Representing Subjective Uncertainty in the CRA-2004 PA — Continued

Sample Position	Variable Name	Material Name	Property Name	Description
34	WSOLAM3S	SOLAM3	SOLSIM	Uncertainty factor (dimensionless) for solubility of Am in the +III oxidation state in Salado brine. Defines UF(Salado, +3, Am) in Equation (90).
35	WSOLAM3C	SOLAM3	SOLCIM	Uncertainty factor (dimensionless) for solubility of Am in the +III oxidation state in Castile brine. Defines UF(Castile, +3, Am) in Equation (90).
36	WSOLPU3S	SOLPU3	SOLSIM	Uncertainty factor (dimensionless) for solubility of Pu in the +III oxidation state in Salado brine. Defines UF(Salado, +3, Pu) in Equation (90).
37	WSOLPU3C	SOLPU3	SOLCIM	Uncertainty factor (dimensionless) for solubility of Pu in the +III oxidation state in Castile brine. Defines UF(Castile, +3, Pu) in Equation (90).
38	WSOLPU4S	SOLPU4	SOLSIM	Uncertainty factor (dimensionless) for solubility of Pu in the +IV oxidation state in Salado brine. Defines UF(Salado, +4, Pu) in Equation (90).
39	WSOLPU4C	SOLPU4	SOLCIM	Uncertainty factor (dimensionless) for solubility of Pu in the +IV oxidation state in Castile brine. Defines UF(Castile, +4, Pu) in Equation (90).
40	WSOLU4S	SOLU4	SOLSIM	Uncertainty factor (dimensionless) for solubility of U in the +IV oxidation state in Salado brine. Defines UF(Salado, +4, U) in Equation (90).
41	WSOLU6S	SOLU6	SOLSIM	Uncertainty factor (dimensionless) for solubility of U in the +VI oxidation state in Salado brine. Defines UF(Salado, +6, U) in Equation (90).
42	WSOLU6C	SOLU6	SOLCIM	Uncertainty factor (dimensionless) for solubility of U in the +VI oxidation state in Castile brine. Defines UF(Castile, +6, U) in Equation (90).
43	WSOLTH4S	SOLTH4	SOLSIM	Uncertainty factor (dimensionless) for solubility of Th in the +IV oxidation state in Salado brine. Defines UF(Salado, +4, Th) in Equation (90).
44	WPHUMOX 3	PHUMOX3	PHUMCIM	Ratio (dimensionless) of concentration of actinides attached to humic colloids to dissolved concentration of actinides for oxidation state +III in Castile brine. Defines SF_{Hum}(Castile, +3, Am) and SF_{Hum}(Castile, +3, Pu) for Equation (90).
45	WOXSTAT	GLOBAL	OXSTAT	Indicator variable for elemental oxidation states (dimensionless). WOXSTAT = 0 indicates use of CMKDPU3, CMKDU4, WSOLPU3C, WSOLPUS, , WSOLU4C, and WSOLU4S. WOXSTAT = 1 implies use of CMKDPU4, CMKDU6, WSOLPU4C, WSOLPU4S, WSOLU6C, and WSOLU6S.

Table PA-17. Variables Representing Subjective Uncertainty in the CRA-2004 PA — Continued

Sample Position	Variable Name	Material Name	Property Name	Description
46	CTRANSFM	CULEBRA	MINP_FAC	Multiplier (dimensionless) applied to transmissivity of the Culebra within the land withdrawal boundary after mining of potash reserves. Defines MF in Equation (216) (see section PA-4.8.2).
47	CTRAN	GLOBAL	TRANSIDX	Indicator variable for selecting transmissivity field. See Section PA-4.8.2.
48	CCLIMSF	GLOBAL	CLIMTIDX	Climate scale factor (dimensionless) for Culebra flow field. Defines SFC in Equation (221).
49	CFRACSP	CULEBRA	HMBLKLT	Culebra fracture spacing (m). Equal to half the distance between fractures (i.e., the Culebra half matrix block length). Defines B in Equation (236) and Figure PA-26.
50	CFRACPOR	CULEBRA	APOROS	Culebra fracture (i.e., advective) porosity (dimensionless). Defines ϕ in Equation (223).
51	CMTRXPOR	CULEBRA	DPOROS	Culebra matrix (i.e., diffusive) porosity (dimensionless). Defines ϕ' in Equation (230).
52	CMKDU6	U+6	MKD_U	Matrix distribution coefficient (m^3/kg) for U in +6 oxidation state. Defines K_{dk} in Equation (231).
53	CMKDU4	U+4	MKD_U	Matrix distribution coefficient (m^3/kg) for U in +4 oxidation state. Defines K_{dk} in Equation (231).
54	CMKDPU3	PU+3	MKD_PU	Matrix distribution coefficient (m^3/kg) for Pu in +3 oxidation state. Defines K_{dk} in Equation (231).
55	CMKDPU4	PU+4	MKD_PU	Matrix distribution coefficient (m^3/kg) for Pu in +4 oxidation state. Defines K_{dk} in Equation (231).
56	CMKDTH4	TH+4	MKD_TH	Matrix distribution coefficient (m^3/kg) for Th in +4 oxidation state. Defines K_{dk} in Equation (231).
57	CMKDAM3	AM+3	MKD_AM	Matrix distribution coefficient (m^3/kg) for Am in +3 oxidation state. Defines K_{dk} in Equation (231).
58	WTAUFAIL	BOREHOLE	TAUFAIL	Shear strength of waste (Pa). Defines $\tau(R,1)$ in Equation (111).
60	PBRINE	GLOBAL	PBRINE	Probability that a drilling intrusion penetrates pressurized brine in the Castile Formation. Defines p_{B1}; see Section PA-3.5.

Table PA-17. Variables Representing Subjective Uncertainty in the CRA-2004 PA — Continued

Sample Position	Variable Name	Material Name	Property Name	Description
61	DOMEGA	BOREHOLE	DOMEGA	Drill string angular velocity (rad/s). Defines $\Delta\Omega$ in Equation (112b).
62	SHURBRN	SHFTU	SAT_RBRN	Residual brine saturation in upper shaft seal materials (dimensionless). Defines S_{br} in Equation (35) for region Upper Shaft in Figure PA-8.
63	SHURGAS	SHFTU	SAT_RGAS	Residual gas saturation in upper shaft seal materials (dimensionless). Defines S_{gr} in Equation (34) for region Upper Shaft in Figure PA-8.
64	SHUPRM	SHFTU	PRMX_LOG	Logarithm of intrinsic permeability (m^2) of upper shaft seal materials. Used in region Upper Shaft in Figure PA-8.
65	SHLPRM1	SHFTL_T1	PRMX_LOG	Logarithm of intrinsic permeability (m^2) of lower shaft seal materials for the first 200 years after closure. Used in region Lower Shaft in Figure PA-8.
66	SHLPRM2	SHFTL_T2	PRMX_LOG	Logarithm of intrinsic permeability (m^2) of lower shaft seal materials from 200 years to 10,000 years after closure. Used in region Lower Shaft in Figure PA-8.
75	RNDSPALL	SPALLMOD	RNDSPALL	Indicator variable for selecting element from the LHS for DRSPALL. See Section PA-4.6.4.

Table PA-18. Differences in Uncertain Parameters in the CCA PA and CRA-2004 PA

Material Name	Property Name	Description	When Used	Reason for Removal or Addition
DRZ_PCS	PRMX_LOG	Logarithm of intrinsic permeability (m^2) of the DRZ immediately above the panel closure concrete.	2003	Added due to the addition of the Option D panel closures.
CONC_PCS	PRMX_LOG	Logarithm of intrinsic permeability (m^2) for the concrete portion of the panel closure.	2003	Added due to the addition of the Option D panel closures.
SOLU4	SOLCIM	Uncertainty factor (dimensionless) for solubility of U in the +IV oxidation state in Castile brine.	2003	Added for completeness.
SOLTH4	SOLCIM	Uncertainty factor (dimensionless) for solubility of Th in the +IV oxidation state in Castile brine.	2003	Added for completeness.

Table PA-18. Differences in Uncertain Parameters in the CCA PA and CRA-2004 PA — Continued

Material Name	Property Name	Description	When Used	Reason for Removal or Addition
DRZ_1	PRMX_LOG	Logarithm of intrinsic permeability (m^2) of the DRZ.	2003	Added from 1997 PAVT (Hansen and Leigh 2003).
CONC_PLG	PRMX_LOG	Logarithm of intrinsic permeability (m^2) of the concrete borehole plugs.	2003	Added from 1997 PAVT (Hansen and Leigh 2003).
GLOBAL	PBRINE	Probability that a drilling intrusion penetrates pressurized brine in the Castile Formation.	2003	Added due to change in Castile Brine pocket modeling (Section 6.12.4.6).
BOREHOLE	DOMEGA	Drill string angular velocity (rad/s).	2003	Added from 1997 PAVT (Hansen and Leigh 2003).
SHFTU	SAT_RBRN	Residual brine saturation in upper shaft seal materials (dimensionless).	2003	Added due to the simplified shaft model.
SHFTU	SAT_RGAS	Residual gas saturation in upper shaft seal materials (dimensionless).	2003	Added due to the simplified shaft model.
SHFTU	PRMX_LOG	Logarithm of intrinsic permeability (m^2) of upper shaft seal materials.	2003	Added due to the simplified shaft model.
SHFTL_T1	PRMX_LOG	Logarithm of intrinsic permeability (m^2) of lower shaft seal materials for the first 200 years after closure.	2003	Added due to the simplified shaft model.
SHFTL_T2	PRMX_LOG	Logarithm of permeability of lower shaft seal materials (m^2) from 200 years to 10,000 years after closure.	2003	Added due to the simplified shaft model.
SPALLMOD	RNDSPALL	Indicator variable for selecting element from the LHS for DRSPALL.	2003	Use of DRSPALL to calculate spall volumes.
CL_L_T1	PRMX_LOG	Logarithm of intrinsic permeability (m^2) for clay components of shaft.	1996	Removed due to the simplified shaft model.
CONC_T1	PRMX_LOG	Logarithm of intrinsic permeability (m^2) for concrete component of shaft seal for 0 to 400 years.	1996	Removed due to the simplified shaft model.
ASPHALT	PRMX_LOG	Logarithm of intrinsic permeability (m^2) for clay components of shaft seal (m^2).	1996	Removed due to the simplified shaft model.
SHFT_DRZ	PRMX_LOG	Logarithm of intrinsic permeability (m^2) of DRZ surrounding shaft.	1996	Removed due to the simplified shaft model.

Table PA-18. Differences in Uncertain Parameters in the CCA PA and CRA-2004 PA — Continued

Material Name	Property Name	Description	When Used	Reason for Removal or Addition
SALT_T1	CUMPROB	Pointer variable used to select intrinsic permeability in crushed salt component of shaft seal at different times.	1996	Removed due to the simplified shaft model.
CASTILER	GRIDFLO	Pointer variable for selection of brine pocket volume.	1996	Removed due to changes in Castile Brine pocket modeling (Section 6.12.4.6).
BLOWOUT	PARTDIA	Waste particle diameter (m).	1996	Removed due to replacement of spall model.

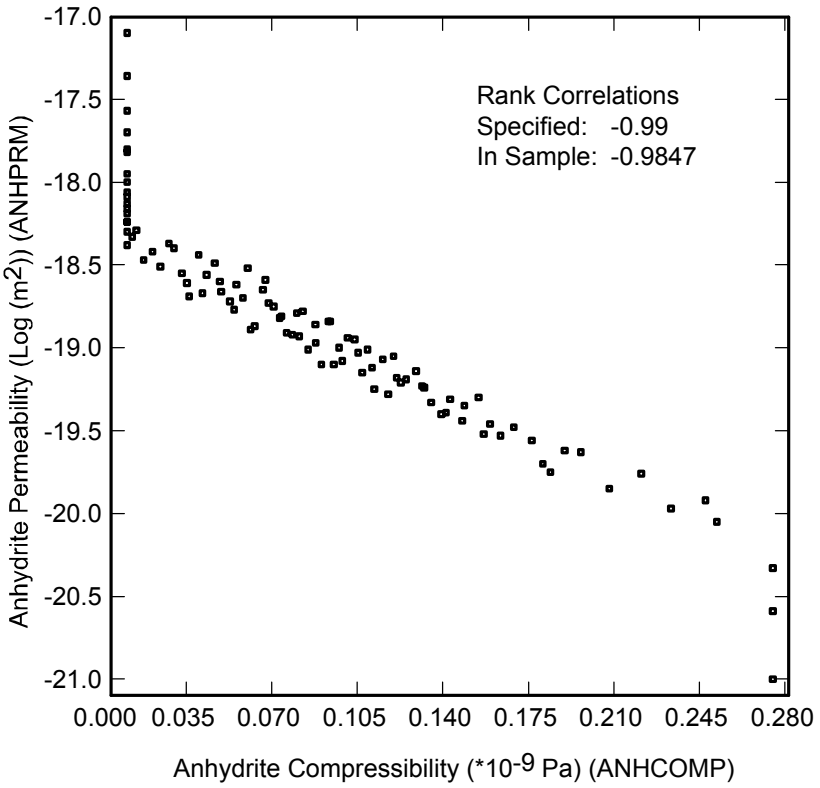

Figure PA-30. Correlation Between ANHCOMP and ANHPRM.

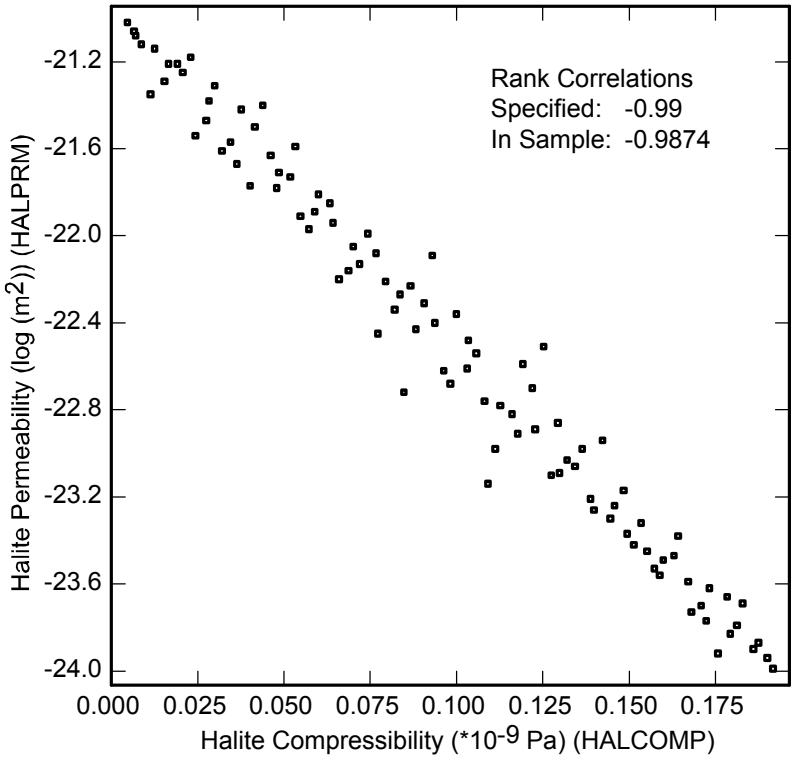

Figure PA-31. Correlation Between HALCOMP and HALPRM.

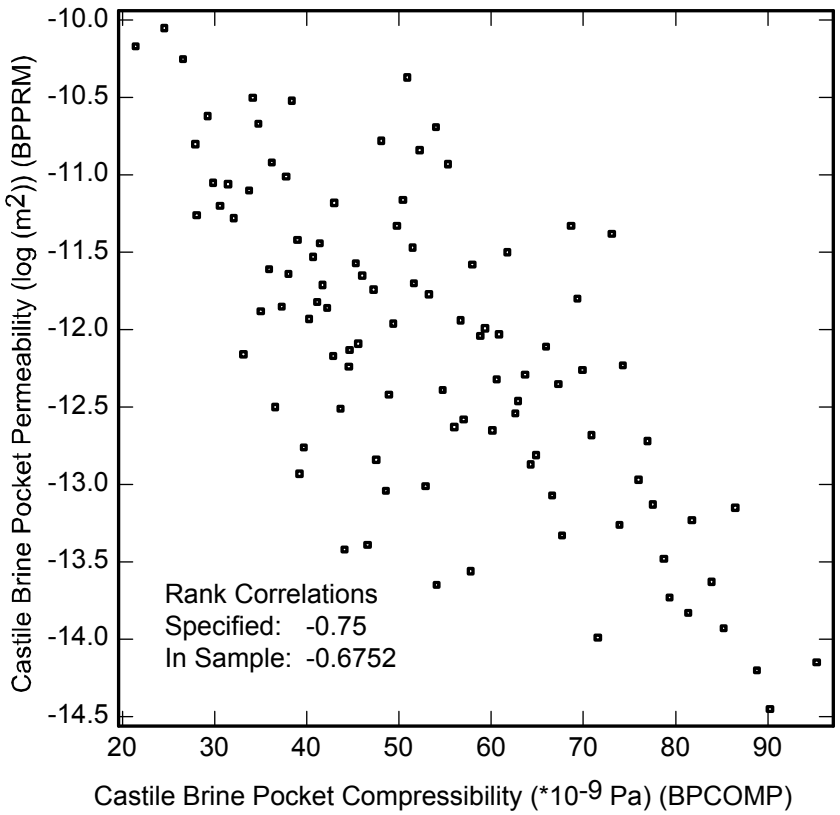

Figure PA-32. Correlation between BPCOMP and BPPRM.

PA-6.0 COMPUTATIONAL PROCEDURES

This section outlines the computational procedures used to execute the CRA-2004 PA. First, this section outlines the sampling procedures applied to evaluate performance accounting for subjective and stochastic uncertainty. The mechanistic calculations used to evaluate the function f in Equation (24) are tabulated, followed by a description of the algorithms used to compute releases. This section concludes with a discussion of sensitivity analysis techniques used to identify which uncertain parameters are primary contributors to the uncertainty in the PA results.

PA-6.1 Sampling Procedures

Extensive use is made of sampling procedures in the CRA-2004 PA. In particular, random sampling is used in the generation of individual CCDFs (i.e., for integration over the probability space (X_{st}, S_{st}, p_{st}) for stochastic uncertainty; see Section PA-2.3) and Latin hypercube sampling is used for the assessment of the effects of imprecisely known analysis inputs (i.e., for integration over the probability space (X_{su}, S_{su}, p_{su}) for subjective uncertainty; see Section PA-2.4).

In random sampling, sometimes also called simple random sampling, the observations

$$\mathbf{x}_k = \left[x_{k1}, x_{k2}, \ldots, x_{knV}\right], \quad k = 1, 2, \ldots, nR, \qquad (255)$$

where nR is the sample size, are selected according to the joint probability distribution for the elements of x as defined by (X_{st}, S_{st}, p_{st}). In practice, (X_{st}, S_{st}, p_{st}) is defined by specifying a distribution D_j for each element x_j of $\mathbf{x}$. Points from different regions of the sample space S_{st}, occur in direct relationship to the probability of occurrence of these regions. Furthermore, each sample element is selected independently of all other sample elements. The random sampling provides unbiased estimates for means, variances, and distributions of the elements $\mathbf{x}$ that comprise (X_{st}, S_{st}, p_{st}).

The random sampling to integrate over the probability space for (X_{st}, S_{st}, p_{st}) for stochastic uncertainty is implemented in the WIPP PA code CCDFGF. The code CCDFGF is capable of generating and evaluating thousands of possible futures; the CRA-2004 PA uses a sample size nS = 10,000 from the space (X_{st}, S_{st}, p_{st}) to estimate repository releases. This sample size is sufficient to estimate the 0.999 quantile of the distribution of releases to the accessible environment.

Latin hypercube sampling is used to integrate over the space for subjective uncertainty (X_{su}, S_{su}, p_{su}). This technique was first introduced by McKay et al (1979). In Latin hypercube sampling, the range of each variable (i.e., the x_j) is divided into nLHS intervals of equal probability and one value is selected at random from each interval. The nLHS values thus obtained for x_1 are paired at random without replacement with the nLHS values obtained

for x_2. These nLHS pairs are combined in a random manner without replacement with the nLHS values of x_3 to form nLHS triples. This process is continued until a set of nLHS nV-tuples is formed. These nV-tuples are of the form

$$\mathbf{x}_k = \left[x_{k1}, x_{k2}, \ldots, x_{knV} \right], \; k = 1, \ldots, nLHS, \qquad (256)$$

and constitute the Latin hypercube sample. The individual x_j must be independent for the preceding construction procedure to work; a method for generating Latin hypercube and random samples from correlated variables was developed by Iman and Conover (1982) and is used in WIPP PA. For more information about Latin hypercube sampling and a comparison with other sampling techniques, see Helton and Davis (2003).

Latin hypercube sampling provides unbiased estimates for means and distribution functions and dense stratification across the range of each sampled variable (McKay et al. 1979), ensuring that the sampled values cover the full range of each uncertain element x_j of $\mathbf{x}$. In particular, uncertainty and sensitivity analysis results obtained with Latin hypercube sampling are robust even when relatively small samples (i.e., nLHS = 50 to 200) are used (Iman and Helton 1988, 1991; Helton et al. 1995).

PA-6.2 Sample Size for Incorporation of Subjective Uncertainty

Section 194.34(d) states that "The number of CCDFs generated shall be large enough such that, at cumulative releases of 1 and 10, the maximum CCDF generated exceeds the 99th percentile of the population of CCDFs with at least a 0.95 probability." For an LHS of size nLHS, the preceding guidance is equivalent to the inequality

$$1 - 0.99^{nLHS} > 0.95, \qquad (257)$$

which results in a minimum value of 298 for nLHS. The CRA-2004 PA uses a total sample size of 300 to integrate over the probability space $\left(X_{su}, S_{su}, p_{su}\right)$ for subjective uncertainty. As discussed in the next section, however, in order to demonstrate convergence of the mean for the population of CCDFs, the total sample of 300 is created by means of three replicated samples of size 100 each.

PA-6.3 Statistical Confidence on Mean CCDF

Section 194.34(f) states that "Any compliance assessment shall provide information which demonstrates that there is at least a 95 percent level of statistical confidence that the mean of the population of CCDFs meets the containment requirements of § 191.13 of this chapter." Given that Latin hypercube sampling is used, the confidence intervals required by Section 194.34(f) are obtained with a replicated sampling technique proposed by Iman (1982). In this technique, the sampling in Equation (256) is repeated nR times with different random seeds. These samples lead to a sequence $\bar{P}_r(R)$, $r = 1, 2, \ldots, nR$, of estimated mean exceedance probabilities, where $\bar{P}_r(R)$ defines the mean CCDF obtained for sample r (i.e., $\bar{P}_r(R)$ is the

mean probability that a normalized release of size R will be exceeded; see Section PA-2.4) and nR is the number of independent samples generated with different random seeds. Then,

$$\bar{P}(R) = \sum_{r=1}^{nR} \bar{P}_r(R) / nR \qquad (258)$$

and

$$SE(R) = \left\{ \sum_{r=1}^{nR} \left[\bar{P}_r(R) - \bar{P}(R) \right]^2 / nR(nR-1) \right\}^{1/2} \qquad (259)$$

provide an additional estimate of the mean CCDF and an estimate of the standard error associated with the mean exceedance probabilities. The t-distribution with nR–1 degrees of freedom can be used to place confidence intervals around the mean exceedance probabilities for individual R values (i.e., around $\bar{P}(R)$). Specifically, the $1-\alpha$ confidence interval is given by $\bar{P}_r(R) \pm t_{1-\alpha/2} SE(R)$, where $t_{1-\alpha/2}$ is the $1-\alpha/2$ quantile of the t-distribution with nR–1 degrees of freedom (e.g., $t_1 - \alpha/2 = 4.303$ for $\alpha = 0.05$ and nR = 3). The same procedure can also be used to place pointwise confidence intervals around percentile curves.

PA-6.4 Generation of LHSs

The LHS program (WIPP PA 1996) is used to produce three independently generated LHSs of size nLHS = 100 each, for a total of 300 sample elements. Each individual replicate is an LHS of the form

$$\mathbf{x}_{su,k} = \left[x_{k1}, x_{k2}, \ldots, x_{knV} \right], \; k = 1, 2, \ldots, nLHS = 100. \qquad (260)$$

In the context of the replicated sampling procedure described in Section PA-6.2, nR = 3 replicates of 100 are used. For notational convenience, the replicates are designated by R1, R2, and R3.

The restricted pairing technique described in Section PA-6.2 is used to induce requested correlations and also to assure that uncorrelated variables have correlations close to zero. The variable pairs (ANHCOMP, ANHPRM), (HALCOMP, HALPRM), and (BPCOMP, BPPRM) are assigned rank correlations of –0.99, –0.99, and –0.75, respectively (Section PA-5.4). All other variable pairs are assigned rank correlations of zero. The restricted pairing technique is very successful in producing these correlations (Table PA-19). Specifically, the correlated variables have correlations that are close to their specified values and uncorrelated variables have correlations that are close to zero.

Table PA-19. Example Correlations in Replicate R1

WGRCOR	1.0000							
WMICDFLG	-0.0993	1.0000						
WGRMICI	0.0152	0.0495	1.0000					
WGRMICH	0.0191	-0.0098	0.0150	1.0000				
WFBETCEL	0.0113	-0.0139	-0.0273	0.0033	1.0000			
WRGSSAT	0.0004	0.0712	-0.0451	-0.0058	-0.0517	1.0000		
WRBRNSAT	0.0192	0.0244	-0.0558	0.0321	-0.0128	-0.0260	1.0000	
WASTWICK	-0.0096	0.0955	-0.0099	0.0043	0.0057	-0.0147	0.0076	1.0000
	WGRCOR	WMICDFLG	WGRMICI	WGRMICH	WFBETCEL	WRGSSAT	WRBRNSAT	WASTWICK

PA-6.5 Generation of Individual Futures

Random sampling (Section PA-6.1) is used to generate elements $\mathbf{x}_{st}$ of S_{st} for CCDF construction. Table PA-20 outlines the algorithm used to generate a single future $\mathbf{x}_{st}$ in the CRA-2004 PA. For each LHS element $\mathbf{x}_{su,k}$, k = 1, 2, …, 300, a total of nS = 10,000 individual futures of the form

$$\mathbf{x}_{st,i} = \left[t_{i1}, e_{i1}, l_{i1}, b_{i1}, p_{i1}, \mathbf{a}_{i1}, t_{i2}, e_{i2}, l_{i2}, b_{i2}, p_{i2}, \mathbf{a}_{i2}, \ldots, t_{in}, e_{in}, l_{in}, b_{in}, p_{in}, \mathbf{a}_{in}, t_{i,min} \right], \quad i = 1, 2, \ldots, nS = 10{,}000 \tag{261}$$

are generated in the construction of all CCDFs for that LHS element. A different random seed is used to initiate the sampling of $\mathbf{x}_{st}$ for each LHS element, with the result that each LHS element uses different values for $\mathbf{x}_{st}$ in CCDF construction. As 300 LHS elements are used in the analysis and 10,000 futures are sampled for each LHS element, the total number of futures $\mathbf{x}_{st}$ used in the analysis in CCDF construction is 3×10^6.

The drilling rate λ_d is used to generate the times at which drilling intrusions occur. For a Poisson process with a constant λ_d (i.e., a stationary process), the CDF for the time Δt between the successive events is given by (Ross 1987, p. 113)

$$prob\left(t \le \Delta t\right) = 1 - \exp\left(-\lambda_d \Delta t\right). \tag{262}$$

A uniformly distributed random number is selected from [0, 1]. Then, solution of

$$r_1 = 1 - \exp\left(-\lambda_d t_1\right) \tag{263}$$

Table PA-20. Algorithm to Generate a Single Future $\mathbf{x}_{st}$ from S_{st}

1. Sample t_1 with a time dependent λ_d given by $\lambda_d(t) = \begin{cases} 0 & \text{if } 0 \le t \le tA \\ \lambda_d & \text{if } t > tA \end{cases}$, *where tA = 100 yr (i.e., time at which administrative control ends) and $\lambda_d = 3.30 \times 10^{-3}\ yr^{-1}$ (see Section PA-3.2).*
2. Sample e_1 with a probability of $pE_0 = 0.797$ that the intrusion will be in an unexcavated area and a probability of $pE_1 = 0.203$ that the intrusion will be in an excavated area (see Section PA-3.3).
3. Sample l_1 with a probability of $pL_j = 6.74 \times 10^{-3}$ for each of the j = 1, 2, …, 144 nodes in Figure PA-6 (see Section PA-3.4).
4. Sample b_1 with a probability of $pB_1 = p(\mathbf{x}_{su})$ that the intrusion will penetrate pressurized brine (see Section PA-3.5).
5. Sample p_1 with probabilities of $pPL_1 = 0.015$, $pPL_2 = 0.696$, and $pPL_3 = 0.289$ that plugging pattern 1, 2, or 3, respectively, will be used (see Section PA-3.6).
6. Sample $\mathbf{a}_1$ (see Section PA-3.7). *6.1 Penetration of nonexcavated area (i.e., $e_1 = 0$): $\mathbf{a}_i = a_1 = 0$.* *6.2 Penetration of excavated area (i.e., $e_1 = 1$): Sample to determine if intrusion penetrates RH-TRU or CH-TRU waste with probabilities of pRH = 0.124 and pCH = 0.876 of penetrating RH-TRU and CH-TRU waste, respectively.* *6.3 Penetration of RH-TRU waste: $\mathbf{a}_i = a_1 = 1$.* *6.4 Penetration of CH-TRU waste: Use probabilities pCH_j of intersecting waste stream j, j = 1, 2, …, 693, (see Attachment PAR, Table PAR-50) to independently sample three intersected waste streams iCH_{11}, iCH_{12}, iCH_{13} (i.e., each of iCH_{11}, iCH_{12}, iCH_{13} is an integer between 1 and 693). Then, $\mathbf{a}_1 = \lfloor 2, iCH_{11}, iCH_{12}, iCH_{13} \rfloor$.*
7. Repeat steps 1 - 6 to determine properties (i.e., t_i, e_i, l_i, b_i, p_i, $\mathbf{a}_i$) of the ith drilling intrusion.
8. Continue until $t_{n+1} > 10{,}000$ yr; the n intrusions thusly generated define the drilling intrusions associated with $\mathbf{x}_{st}$.
9. Sample t_{min} with a time dependent λ_m given by $\lambda_m(t) = \begin{cases} 0 & \text{if } 0 \le t \le tA \\ \lambda_m & \text{if } t > tA \end{cases}$ *where tA = 100 yr and $\lambda_m = 1 \times 10^{-4}\ yr^{-1}$ (see Section PA-3.8).*

for t_1 gives the time of the first drilling intrusion. An initial period of 100 years of administrative control is assumed, thus 100 years is added to the t_1 obtained in Equation (263) to obtain the time of the first drilling intrusion. Selection of a second random number r_2 and solution of

$$r_2 = 1 - \exp(-\lambda_d \Delta t_1) \qquad (264)$$

for Δt_1 gives the time interval between the first and second drilling intrusions, with the outcome that $t_2 = t_1 + \Delta t_1$. This process is continued until t_{n+1} exceeds 10,000 yr. The times $t_1, t_2, \ldots, t_n$ then constitute the drilling times in $\mathbf{x}_{st}$ in Equation (261).

The mining time t_{min} is sampled in a manner similar to sampling the drilling times. Additional uniformly distributed random numbers from $[0,1]$ are used to generate the elements e_i, l_i, b_i, p_i, $\mathbf{a}_i$ of $\mathbf{x}_{st}$ from their assigned distributions (see Section PA-3.0).

PA-6.6 Construction of CCDFs

In the CRA-2004 PA, the sampling of individual futures (Section PA-6.5) and associated CCDF construction is carried out by the CCDFGF program (WIPP PA 2003d). The sampled futures $\mathbf{x}_{st,i}$ in Equation (261) are used to construct CCDFs for many different quantities (e.g., cuttings and cavings releases, spallings releases, direct brine releases, etc.). The construction process is the same for each quantity. For notational convenience, assume that the particular quantity under consideration can be represented by a function $f\left(\mathbf{x}_{st,i}\right)$, with the result that 10,000 values

$$f\left(\mathbf{x}_{st,i}\right),\ i = 1, 2, \ldots, 10{,}000 \qquad (265)$$

are available for use in CCDF construction. Formally, the resultant CCDF is defined by the expression in Equation (4). In practice, the indicator function δ_R is not directly used and the desired CCDF is obtained after an appropriate ordering of the $f\left(\mathbf{x}_{st,i}\right)$ (i.e., from smallest to largest or largest to smallest) as described below.

The CRA-2004 PA uses a binning procedure in CCDF construction to simplify sorting the individual $f\left(\mathbf{x}_{st,i}\right)$ and to reduce the number of plot points. Specifically, the range of f is divided into intervals (i.e., bins) by the specified points

$$f_{min} = b_0 < b_1 < b_2 < \ldots < b_n = f_{max}, \qquad (266)$$

where f_{min} is the minimum value of f to be plotted (typically 10^{-6} or 10^{-5} when an EPA normalized release is under consideration), f_{max} is the maximum value of f to be plotted (typically 100 when an EPA normalized release is under consideration), n is the number of bins in use, and the b_i are typically loguniformly placed with 20 values per order of magnitude. A counter nB_j is used for each interval $\left[b_{j-1}, b_j\right]$. All counters are initially set to zero. Then, as individual values $f\left(\mathbf{x}_{st,i}\right)$ are generated, the counter nB_j is incremented by 1 when the inequality

$$b_{j-1} < f\left(\mathbf{x}_{st,i}\right) \le b_j \tag{267}$$

is satisfied. When necessary, f_{max} is increased in value so that the inequality $f\left(\mathbf{x}_{st,i}\right) < f_{max}$ will always be satisfied. Once the 10,000 values for $f\left(\mathbf{x}_{st,i}\right)$ have been generated, a value of nB_j exists for each interval $\left[b_{j-1}, b_j\right]$. The quotient

$$pB_j = nB_j / 10{,}000 \tag{268}$$

provides an approximation to the probability that $f\left(\mathbf{x}_{st}\right)$ will have a value that falls in the interval $\left[b_{j-1}, b_j\right]$. The resultant CCDF is then defined by the points

$$\left(b_j, prob\left(value > b_j\right)\right) = \left(b_j, \sum_{k=j+1}^{n} pB_k\right) \tag{269}$$

for j = 0, 1, 2, …, n–1, where $prob\left(value > b_j\right)$ is the probability that a value greater than b_j will occur.

The binning technique produces histograms that are difficult to read when multiple CCDFs appear in a single plot. As the number of futures is increased and the bins are refined, the histogram CCDF should converge to a continuous CCDF as additional points (i.e., elements $\mathbf{x}_{st}$ of S_{st}) are used in its construction. The continuous CCDF is approximated by drawing diagonal lines from the left end of one bin to the left end of the next bin.

When multiple CCDFs appear in a single plot, the bottom of the plot becomes very congested as the individual CCDFs drop to zero on the abscissa. For this reason, each CCDF stops at the largest observed consequence value among the 10,000 values calculated for that CCDF. Stopping at the largest consequence value rather than the left bin boundary of the bin that contains this value permits the CCDF to explicitly show the largest observed consequence. Due to the use of a sample size of 10,000 in the generation of CCDFs for comparison with the EPA release limits, the last nonzero exceedance probability in the resultant CCDFs is typically 10^{-4}; Figure PA-5 shows an example of CCDFs from the 2004 PA.

PA-6.7 Mechanistic Calculations

For the CRA-2004 PA, calculations were performed with the models described in Chapter PA-4.0 for selected elements of S_{st} (see Section PA-3.9) and the results were used to determine the releases to the accessible environment for the large number (i.e., 10,000) of randomly sampled futures used in the estimation of individual CCDFs. The same set of mechanistic calculations was performed for each LHS element. This section summarizes the calculations performed with each of the models described in Chapter PA-4.0; Section PA-6.8 outlines the algorithms

used to construct releases for the randomly sampled elements $\mathbf{x}_{st,i}$ of S_{st} from the results of the mechanistic calculations. Long (2003) documents execution of the calculations and archiving of calculation results.

PA-6.7.1 BRAGFLO Calculations

The BRAGFLO code (Section PA-4.2) computes two-phase (brine and gas) flow in and around the repository. BRAGFLO results are used as initial conditions in the models for Salado Transport (implemented in NUTS and PANEL), spallings (implemented in CUTTINGS_S) and DBR (also calculated by BRAGFLO). Thus, the BRAGFLO scenarios are used to define scenarios for other codes.

The four fundamental scenarios for the CRA-2004 PA (Section PA-3.9) define four categories of calculations to be performed with BRAGFLO (i.e., E0, E1, E2, and E1E2). These four fundamental scenarios were expanded into six general scenarios by specifying the time of drilling intrusions. Table PA-21 summarizes the specific scenarios used in the CRA-2004 PA. A total of 6 scenarios × nR × nLHS = 6 × 3 × 100 = 1800 BRAGFLO calculations were conducted for the CRA-2004 PA.

Table PA-21. BRAGFLO Scenarios in the CRA-2004 PA

Fundamental Scenario (Section PA-3.9)	Specific Scenario	Time of drilling intrusion(s)
E0: no drilling intrusions	S1	N/A
E1: single intrusion into excavated area ($e_1 = 1$), pressurized brine is penetrated ($b_1 = 1$), and plugging pattern 2 is used ($p_1 = 2$).	S2	350 years
	S3	1,000 years
E2: single intrusion into excavated area ($e_1 = 1$), pressurized brine is penetrated ($b_1 = 1$) and plugging pattern 3 is used ($p_1 = 3$), or pressurized brine is not penetrated ($b_1 = 0$).	S4	350 years
	S5	1,000 years
E1E2: two intrusions into the same waste panel ($e_1 = e_2 = 1$), the first being an E2 intrusion and the second being an E1 intrusion.	S6	800 years for E2 intrusion 2,000 years for E1 intrusion

Values for the activity level $\mathbf{a}_1$ and for mining time t_{min} are not needed for the mechanistic calculations; these values are used in the construction of the releases from the results of the mechanistic calculations (Section PA-6.8). Although a value for drilling location l_1 is not specified, a drilling location is required for the BRAGFLO calculations. If equivalent grids were used in the definition of $\mathbf{x}_{st}$ (Figure PA-6) and in the numerical solution of the partial differential equations on which BRAGFLO is based (Figure PA-8), the location of the drilling intrusion used in the BRAGFLO calculations could be specified as a specific value for l_1, which in turn would correspond to one of the 144 locations in Figure PA-6 that are designated by l in the definition of $\mathbf{x}_{st}$. However, as these grids are not the same, a unique pairing

between a value for l_1 and the location of the drilling intrusion used in the computational grid employed with BRAGFLO is not possible. The BRAGFLO computational grid divides the repository into a lower waste panel (area Waste Panel), a middle group of four waste panels (area South RoR), and an upper group of five waste panels (area North RoR), with the drilling intrusion taking place through the center of the lower panel (Figure PA-8). Thus, in the context of the locations in Figure PA-6 potentially indexed by l_1, the drilling intrusions in Scenario S2, Scenario S3, Scenario S4 and Scenario S5 occur at a location in Panel 5. In Scenario S6, both intrusions occur at a location in Panel 5, with the effects of flow between the two boreholes implemented through assumptions involving the time-dependent behavior of borehole permeability (Table PA-5).

PA-6.7.2 NUTS Calculations

Transport through the Salado is computed by the code NUTS (Section PA-4.3) using the flow fields computed by BRAGFLO. Two types of calculations are performed with NUTS. First, a set of screening calculations identifies elements of the sample from S_{su} for which radionuclide transport is possible through the Salado to the LWB or to the Culebra. The screening calculations identify a subset of the sample from S_{st} for which transport is possible and for which releases calculations are performed. Screening calculations are performed for all BRAGFLO cases, for a total of 1500 screening calculations with NUTS (Table PA-21). Table PA-22 summarizes the NUTS release calculations for the CRA-2004 PA. Based on the screening calculations, a total of 1402 release calculations are performed for the CRA-2004 PA. For each vector that is retained (based on the screening calculations), release calculations are performed for a set of intrusion times.

Table PA-22. NUTS Release Calculations in the CRA-2004 PA

NUTS Scenario	Number of vectors (all replicates)	Flow field	Intrusion time (t_1)
S1	1 + 0 + 0 = 1	BRAGFLO S1 scenario	N/A
S2	60 + 64 + 61 = 185	BRAGFLO S2 scenario	E1 intrusion at 100 and 350 years
S3	49 + 55 + 51 = 155	BRAGFLO S3 scenario	E1 intrusion at 1,000, 3,000, 5,000, 7,000 and 9,000 years
S4	13 + 14 + 11 = 38	BRAGFLO S4 scenario	E2 intrusion at 100, 350 years
S5	12 + 13 + 11 = 36	BRAGFLO S5 scenario	E2 intrusion at 1,000, 3,000, 5,000, 7,000 and 9,000 years

Table PA-22 lists five scenarios for release calculations corresponding to the five BRAGFLO scenarios. Each NUTS scenario uses the flow field computed for the corresponding BRAGFLO scenario. The intrusion times for the NUTS scenarios are accommodated by shifting the BRAGFLO flow fields in time so that the NUTS and BRAGFLO intrusions coincide. For example, the NUTS S3 scenario with an intrusion at 3,000 years requires a flow field for the time interval between (3,000 yr, 10,000 yr); this scenario uses the BRAGFLO S3 flow field for the time interval between (1,000 yr, 8,000 yr).

Values for the variables indicating intrusion into excavated area (e_1), penetration of pressurized brine (b_1), plugging pattern (p_1) and drilling location (l_1) are the same as in the corresponding BRAGFLO scenario. Values for the activity level $\mathbf{a}_i$ and for mining time t_{min} are not specified for the NUTS scenarios.

PA-6.7.3 PANEL Calculations

As outlined in Section PA-4.4, the code PANEL is used to estimate releases to the Culebra associated with E1E2 scenarios and to estimate radionuclide concentrations in brine for use in the estimation of direct brine releases. An E1E2 scenario assumes two drilling intrusions into the same waste panel: the first intrusion being an E2 intrusion (Table PA-22) occurring at time t1 and the second intrusion being an E1 intrusion (Table PA-22) occurring at time t_2. PANEL calculations are performed for t_2 = 100, 350, 1,000, 2,000, 4,000, 6,000 and 9,000 years using the flow field produced by the single BRAGFLO calculation for Scenario S6, for a total of 7 × nR × nLHS = 7 × 3 × 100 = 2100 PANEL calculations. The BRAGFLO flow field is shifted forward or backward in time as appropriate so that the time of the second intrusion (t_2) coincides. The shifting of the BRAGFLO flow field results in values for the time (t_1) of the first intrusion (E2) for the PANEL calculations given by

$$t_1 = \max\left\{100\,yr,\ t_2 - 1200\,yr\right\}, \qquad (270)$$

where the restriction that t_1 cannot be less than 100 years results from the definition of $\mathbf{x}_{st}$, which does not allow negative intrusion times, and from the assumption of 100 years of administrative control during which there is no drilling (i.e., $\lambda_d(t) = 0\ yr^{-1}$ for $0 \le t \le 100\ yr$; see Equation (7)). Under this convention, what is specified in concept by the definition of Scenario S6 for the BRAGFLO calculations differs from what is actually done computationally because t_1 does not always precede t_2 by 1200 yr in the PANEL calculation. Values for the other variables defining the element $\mathbf{x}_{st}$ of S_{st} for the PANEL E1E2 scenarios are the same as in the BRAGFLO S6 scenario.

Calculation of radionuclide concentration are not specific to any BRAGFLO scenario. The concentration calculations compute the mobilized activity in two different brines (Castile and Salado) and are performed at 100, 125, 175, 350, 1,000, 3,000, 5,000, 7,500 and 10,000 years for a total of 2 × 9 × nR = 54 calculations.

PA-6.7.4 CUTTINGS_S Calculations

The code CUTTINGS_S computes the volumes of solids removed from the repository by cuttings and cavings (see Section PA-4.5) and spallings (see Section PA-4.6). Table PA-23 lists the CUTTINGS_S calculations performed for the CRA-2004 PA, totaling 78 × nR × nLHS = 78 × 3 × 100 = 23,400 CUTTINGS_S calculations.

Table PA-23. CUTTINGS_S Scenarios in the CRA-2004 PA

Scenario	*Description*
S1	*Intrusion into lower, middle, and upper waste panel in undisturbed (i.e., E0 conditions) repository at 100, 350, 1,000, 3,000, 5,000, and 10,000 years = 18 combinations.*
S2	*Initial E1 intrusion at 350 years followed by a second intrusion into the same, adjacent, and nonadjacent waste panel at 550, 750, 2,000, 4,000 or 10,000 years = 15 combinations.*
S3	*Initial E1 intrusion at 1000 years followed by a second intrusion into the same, adjacent, and nonadjacent waste panel at 1200, 1,400, 3,000, 5,000 or 10,000 years = 15 combinations.*
S4	*Initial E2 intrusion at 350 years followed by a second intrusion into the same, adjacent, and nonadjacent waste panel at 550, 750, 2,000, 4,000 or 10,000 years = 15 combinations.*
S5	*Initial E2 intrusion at 1000 years followed by a second intrusion into the same, adjacent, and nonadjacent waste panel at 1,200, 1,400, 3,000, 5,000 or 10,000 years = 15 combinations.*

The CUTTINGS_S S1 scenario computes volumes of solid material released from the initial intrusion in the repository. Initial conditions for the CUTTINGS_S S1 scenario are taken from the results of the BRAGFLO S1 scenario at the time of the intrusion for areas Waste Panel, South RoR, and North RoR in Figure PA-8, corresponding to the lower, middle, and upper waste panels. In this scenario, the excavated area is penetrated ($e_1 = 1$) and the drilling location (l_1) is defined as one of the nodes (Figure PA-6) in the appropriate panel of Figure PA-20. The actual locations at which the intrusions are assumed to occur correspond to the points in Figure PA-20 designated "Down-dip well," "Middle well," and "Up-Dip Well" for the lower, middle, and upper waste panel, respectively. Values for the variables indicating penetration of pressurized brine (b_1), plugging pattern (p_1), activity level (a_1), and for mining time (t_{min}) are not specified for the CUTTINGS_S S1 scenario.

The other CUTTINGS_S scenarios (Scenario S2, Scenario S3, Scenario S4, and Scenario S5) compute volumes of solids released by a second or subsequent intrusion. Initial conditions are taken from the results of the corresponding BRAGFLO scenario at the time of the second intrusion. As in the BRAGFLO scenarios, the first intrusion occurs in the lower waste panel (area Waste Panel in Figure PA-8) so the drilling location (l_1) is defined as one of the nodes in Panel 5 (Figure PA-6). The second intrusion occurs in the same waste panel as the first intrusion (area Waste Panel in Figure PA-8), an adjacent waste panel (area South RoR in Figure PA-8), or a nonadjacent waste panel (area North RoR in Figure PA-8). Hence the drilling location (l_2) is defined as one of the nodes (Figure PA-6) in the appropriate panel of Figure PA-20.

The activity level for the first intrusion a_1 takes a value that indicates penetration of CH-TRU waste (i.e., $a_1 = [2, CH_{11}, CH_{12}, CH_{13}]$) but the specific waste streams penetrated (i.e. CH_{11}, CH_{12}, CH_{13}) are not specified. For the second intrusion, the excavated area is penetrated

(e_2 = 1) and the drilling location (l_2) is defined as one of the nodes (Figure PA-6) in the appropriate panel, as described above. The actual locations at which the intrusions are assumed to occur correspond to the point in Figure PA-20 designated "Down-dip well" for the first intrusion for Category (1) intrusions and "Up-dip well, first or second intrusion" for Category (2) intrusions. As for the first intrusion, the activity level a_2 only indicates penetration of CH-TRU waste. Values for the other variables defining the first intrusion (e_1, b_1, and p_1) are the same as in the corresponding BRAGFLO scenario. Values for the other variables defining the second intrusion (b_2 and p_2) and the mining time t_{min} are not specified for the CUTTINGS_S scenarios.

PA-6.7.5 BRAGFLO Calculations for Direct Brine Release Volumes

Volumes of brine released to the surface at the time of an intrusion are calculated using BRAGFLO as described in Section PA-4.7. Calculations of DBR volumes were conducted for the same scenarios as for CUTTINGS_S (Table PA-23). Thus, the elements of S_{st} described in Section PA-6.7.4 also characterize the elements of S_{st} for which DBR volumes are computed; a total of 23,400 BRAGFLO calculations were performed.

PA-6.7.6 MODFLOW Calculations

As described in Section PA-4.8, the MODFLOW calculations produce flow fields in the Culebra for two categories of conditions: partially-mined conditions in the vicinity of the repository and fully-mined conditions in the vicinity of the repository (Figure PA-23). As specified in 40 CFR § 194.32(b), partially-mined conditions are assumed to exist by the end of the period of administrative control (i.e., at 100 years after closure). After the time that mining occurs within the LWB (t_{min}; see Section PA-3.8), fully-mined conditions are assumed for the remainder of the 10,000 regulatory period. The flow fields for partially-mined conditions are calculated by MODFLOW using the t-fields for partially-mined conditions (see Section PA-4.8.2). Additional MODFLOW calculations determine the flow fields for fully-mined conditions and are performed using the t-fields for fully-mined conditions. Thus a total of 2 × nR × nLHS = 2 × 3 × 100 = 600 MODFLOW calculations were performed. The element CTRAN of x_{su} (see Table PA-17) specifies the association between the uncertain transmissivity fields and the calculation of flow fields by MODFLOW.

Table PA-24. MODFLOW Scenarios in the CRA-2004 PA

MODFLOW: 600 Flow-Field Calculations
PM: Partially mined conditions in vicinity of repository
FM: Fully mined conditions in vicinity of repository
Total calculations = 2 nR nLHS = 2 × 3 × 100 = 600
Note: Only 100 unique transmissivity fields were constructed with MODFLOW for use in the analysis. The transmissivity fields are an input to the calculation of flow-fields. In each replicate, the transmissivity field used for a particular flow field was assigned using an index value (CTRAN, see Table PA-17) included in the LHS.

PA-6.7.7 SECOTP2D Calculations

The SECOTP2D calculations are performed for the same elements $\mathbf{x}_{st,0}$ and $\mathbf{x}_{st,m}$ of S_{st} defined in Section PA-6.7.6 for the MODFLOW calculations for a total of $2 \times nR \times nLHS = 2 \times 3 \times 100 = 600$ SECOTP2D calculations.

Table PA-25. SECOTP2D Scenarios in the CRA-2004 PA

SECOTP2D: 600 Calculations
PM: Partially mined conditions in vicinity of repository
FM: Fully mined conditions in vicinity of repository
Total calculations = 2 nR nLHS = 2 × 3 × 100 = 600
Note: Each calculation includes a unit release of each of four radionuclides: ^{241}Am, ^{239}Pu, ^{230}Th, ^{234}U.

PA-6.8 Computation of Releases

The mechanistic computations outlined in Section PA-6.7 are used to compute releases for each sampled element $\mathbf{x}_{st}$ of S_{st}. Releases from the repository can be partitioned into three categories: undisturbed releases, which may occur in futures without drilling intrusions; direct releases, which occur at the time of a drilling event; and long-term releases, which occur as a consequence of a history of drilling intrusions. For a given future ($\mathbf{x}_{st}$ of S_{st} in Equation (261)) other than undisturbed conditions ($\mathbf{x}_{st,0}$) the direct and long-term releases are computed by the code CCDFGF (WIPP PA 2003a) from the results of the mechanistic calculations summarized in Section PA-6.7, performed with the models presented in Chapter PA-4.0. Releases from an undisturbed repository are computed from the results of the NUTS S1 scenario (Section PA-6.7.2).

PA-6.8.1 Undisturbed Releases

Releases from the repository for the futures ($\mathbf{x}_{st,0}$) in which no drilling intrusions occur are computed by the NUTS release calculations for E0 conditions (Table PA-22). The NUTS model computes the activity of each radionuclide that reaches the accessible environment during the regulatory period via transport through the MBs and through the Dewey Lake Red Beds. These releases are represented as $f_{MB}\left[\mathbf{x}_{st,0}, f_B\left(\mathbf{x}_{st,0}\right)\right]$ and $f_{DL}\left[\mathbf{x}_{st,0}, f_B\left(\mathbf{x}_{st,0}\right)\right]$ in Equation (24).

PA-6.8.2 Direct Releases

Direct releases include cuttings, cavings, spallings, and DBRs. The model for each component of direct releases computes a volume (solids or liquid) released to directly to the surface for each drilling intrusion. These volumes are combined with an appropriate concentration of activity in the released waste.

PA-6.8.3 Construction of Cuttings and Cavings Releases

Each drilling intrusion encountering waste is assumed to release a volume of solid material as cuttings as described in Section PA-4.5.2. The uncompacted volume of waste removed by cuttings (V_{cut}) is computed by Equation (104). In addition, drilling intrusions that encounter CH-TRU waste may release additional solid material as cavings, as described in Section PA-4.5.2. The uncompacted volume of material removed by cuttings and cavings combined ($V = V_{cut} + V_{cav}$) is computed by Equation (105). For a drilling intrusion that encounter RH-TRU waste, the final eroded diameter D_f in Equation (105) is equal to the bit diameter in Equation (104). In the CRA-2004 PA, all drilling intrusions assume a drill bit diameter of 12.25 in (Attachment PAR, Table PAR-13).

The uncompacted volume of material removed is not composed entirely of waste material; rather, the uncompacted volume includes MgO and any void space initially present around the waste containers. The volume of waste removed (V_w) is determined by multiplying the uncompacted volume by the fraction of excavated volume (FVW) of the repository that is occupied by waste. In the CRA-2004 PA, FVW = 0.386 for CH-TRU waste and FVW = 1.0 for RH-TRU waste (Attachment PAR, Table PAR-45), thus

$$V_w = V \times FVW \,. \qquad (271)$$

The activity in the material released by cuttings and cavings is determined by stochastically selecting a subset of the set of all waste streams. The vector ($\mathbf{a}_i$) described in Section PA-3.7 determines which type of waste (CH-TRU or RH-TRU) and which waste streams are selected. The activity per m^3 of waste stream volume is computed for each waste stream at a discrete set of times by the code EPAUNI (Fox 2003), the results of the EPAUNI calculations are presented in Attachment PAR, Tables PAR-50 through PAR-61. Activities at other times are determined by linear interpolation. The cuttings and cavings release $f_C(\mathbf{x}_{st})$ is the product of the average activity per m^3 (C_r, computed as the average activity over the waste streams comprising the selected subset with the assumption that each waste stream contributes an equal volume to the release) and the volume of waste released (Equation (272)).

$$f_C(\mathbf{x}_{st}) = V_w \times C_r \,. \qquad (272)$$

PA-6.8.4 Determining Initial Conditions for Direct and Transport Releases

A sequence of intrusions into the repository can change the conditions in and around the repository and hence affect releases from subsequent intrusions. This section describes how panel and repository conditions are determined for a given intrusion.

PA-6.8.4.1 <u>Determining Repository and Panel Conditions</u>

Direct releases by DBR and spallings, and subsequent releases by radionuclide transport require a determination of the conditions in the intruded panel and in the repository at the time of the intrusion. One of three conditions is assigned to the repository:

E0 ***the repository is undisturbed by drilling,***

E1 ***the repository has at least one E1 intrusion, or***

E2 ***the repository has one or more E2 intrusions but no E1 intrusions.***

In addition, each panel is assigned one of four conditions:

E0 ***the excavated regions of the panel have not been intruded by drilling,***

E1 ***the panel has one previous E1 intrusions (intersects a brine reservoir in the Castile),***

E2 ***the panel has one or more previous E2 intrusions (none intersect brine reservoirs), or***

E1E2 ***the panel has at least two previous intrusions, at least one of which is an E1 intrusion.***

Repository conditions are used to determine direct releases for each intrusion by DBRs and spallings. Panel conditions are used to determine releases by transport through the Culebra.

When an intrusion into CH-TRU waste occurs, the stochastic variables in Table PA-20 are used in the algorithm shown in Figure PA-33 to determine the type of the intrusion (E1 or E2). The type of the intrusion is used to update the conditions for the intruded panel and the repository before stepping forward in time to the next intrusion.

PA-6.8.4.2 Determining Distance from Previous Intrusions

Direct releases by DBR and spallings require a determination of the distance between the panel hit by the current intrusion and the panels hit by previous intrusions. In the CRA-2004 PA, the 10 panels are divided into three groups: lower, consisting of only panel 5; middle, including of panels 3, 4, 6, and 9; and upper, including of panels 1, 2, 7, 8, and 10, as shown in Figure PA-21. These divisions are consistent with the representation of the repository in the BRAGFLO model for Salado flow (Section PA-4.2) and for DBRs (Section PA-4.7).

Although the initial intrusion can occur in any of the 10 actual waste panels, direct releases for the initial intrusion are modeled as if the initial intrusion occurred in a lower waste panel (panel 4 or 5; see Figure PA-6), by using initial conditions for direct releases from the waste panel in the BRAGFLO grid (Figure PA-8), which are mapped to the lower panel in Figure PA-21. This treatment is the same as in the CCA PA and is conservative, since the waste panel typically has higher brine saturation than do the panels in the rest of repository areas (see Sections PA-7.1.2 and PA-8.3.2). Initial conditions for direct releases from subsequent intrusions are modeled by one of three cases: lower, middle, and upper, corresponding to the three panel groups shown in Figure PA-21 and listed in Table PA-24. The lower case represents a second intrusion into a previously intruded panel. The middle case represents an intrusion into an undisturbed

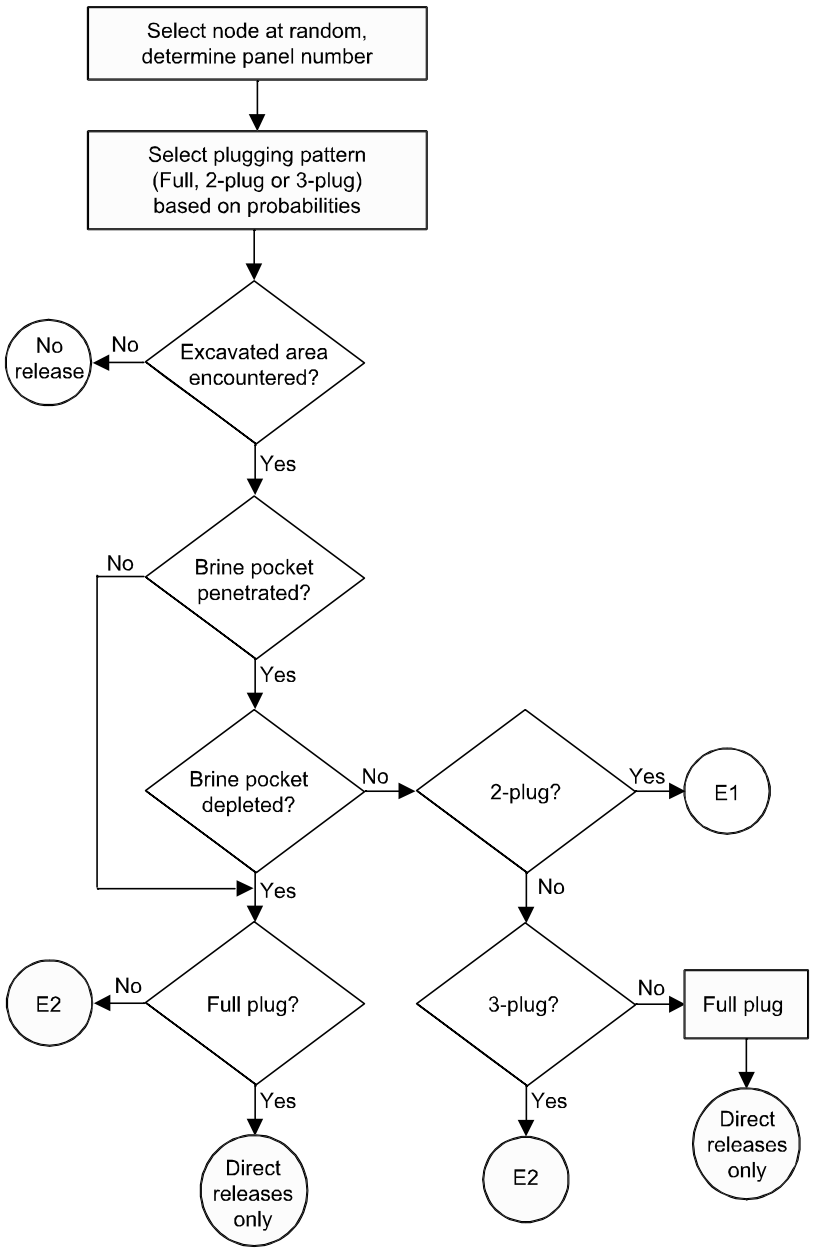

Figure PA-33. The Determination of the Type of Intrusion.

panel that is adjacent to a previously disturbed panel. The upper case represents an intrusion into an undisturbed panel that is not adjacent to a previously disturbed panel. Adjacent panels share one side in common and nonadjacent panels share no sides in common.

Selection of the time and location of the previous intrusion used to determine distance from the current intrusion depends on the repository condition. The repository condition is determined by the intrusion of greatest consequence across all panels prior to the current intrusion. E1 intrusions are assumed to be of the greater consequence than E2 intrusions. The previous intrusion is selected by finding the closest panel (same, adjacent, nonadjacent) whose intrusion condition, excluding the current intrusion, is equal to the repository

condition. The time of the previous intrusion is the time of the most recent intrusion having the greatest consequence and closest distance. Likewise, the condition of each panel is equal to the intrusion of greatest consequence into the panel prior to the current intrusion.

PA-6.8.5 Construction of Direct Brine Releases

DBRs (also termed blowout releases) are calculated for all intrusions that encounter CH-TRU waste. DBRs $f_{DBR}(\mathbf{x}_{st})$ are constructed from volume of brine released (V_{DBR}) to the surface (Equation (175)) and radionuclide concentrations in brine (C_{bl}, see Equation (85)). Brine volume released to the surface is computed by BRAGFLO (Section PA-4.7.3) for the times listed in Table PA-23; brine volumes released for intrusions at other times are computed by linear interpolation (WIPP PA 2003d).

Calculation of DBR volumes distinguishes between the first intrusion and subsequent intrusions. The release volumes for the initial intrusion (E0 repository conditions) are further distinguished by the panel group (upper, middle, and lower). As shown in Table PA-23, BRAGFLO computes release volumes for the initial intrusion at each of a series of intrusion times; the release volume for the initial intrusion at other times is computed by linear interpolation (WIPP PA 2003a). Release volumes for subsequent intrusions are distinguished by the current state of the repository (E1 or E2) and the relative distance between the panel intruded by the current borehole and the panel of the initial intrusion (same, adjacent, non-adjacent). The algorithms for determining repository conditions and distance between intrusions are described in Section PA-6.8.4.

As indicated in Table PA-23, DBR volumes for a second intrusion are computed by BRAGFLO for a set of combinations of repository condition, distance between intrusions, and time between intrusions. Brine release volumes for other combinations of condition, distance, and time are computed by linear interpolation (WIPP PA 2003a). Brine releases from third and subsequent intrusions are computed as if the current intrusion was the second intrusion into the repository.

Radionuclide concentrations in brine (C_{bl}) are calculated by PANEL (Section PA-6.7.3) for the times listed in Table PA-22; concentrations at other times are computed by linear interpolation (WIPP PA 2003a). The type of intrusion (E1 or E2) determines the brine (Salado or Castile brine) selected for the concentration calculation; for E1 intrusions, Castile brine is used, and Salado brine is used for E2 intrusions.

The direct brine release is computed as the product of the release concentration and the volume, V_{DBR}, i.e.

$$f_{DBR}(\mathbf{x}_{st}) = V_{DBR} \times C_{bl} \qquad (273)$$

PA-6.8.6 Construction of Spallings Releases

Spallings releases are calculated for all intrusions that encounter CH-TRU waste. The construction of the spallings release $f_{SP}(\mathbf{x}_{st})$ is nearly identical to that described in Section

PA-6.8.5 for the calculation of DBRs except that volumes of solid material released will be used rather than volumes of brine. These solid releases are calculated with the spallings submodel of the CUTTINGS_S program for the combinations of repository condition, distance from previous intrusions, and time between intrusions listed in Table PA-23. Linear interpolation determines the releases for other combinations of repository condition, distance, and time between intrusions (WIPP PA 2003a).

The concentration of radionuclides in the spallings release volume is computed as the average activity per m^3 in the CH-TRU waste at the time of intrusion. Activities in each waste stream are computed at a discrete set of times by the code EPAUNI (Fox 2003); activities at other times are determined by linear interpolation.

PA-6.8.7 Radionuclide Transport Through the Culebra

One potential path for radionuclide transport from the repository is up through boreholes to the Culebra, then through the Culebra to the LWB (Section 6.4.6). As indicated in Table PA-22, the NUTS and PANEL models are used to estimate radionuclide transport through boreholes to the Culebra $f_{NP}(x_{st})$ for a fixed set of intrusion times; releases to the Culebra for intrusions at other times are determined by linear interpolation (WIPP PA 2003a). NUTS computes the release to the Culebra over time for E1 and E2 boreholes; PANEL computes the release to the Culebra for an E1E2 borehole.

Each borehole may create a pathway for releases to the Culebra. The first E1 or E2 borehole in each panel creates a release path, with the radionuclide release taken from the appropriate NUTS data. Subsequent E2 boreholes into a panel with only E2 boreholes do not cause additional releases; WIPP PA assumes that a subsequent E2 borehole into a panel having only earlier E2 intrusions does not provide a significant source of additional brine, and thus does not release additional radionuclides to the Culebra.

An E1E2 borehole results from the combination of two or more intrusions into the same panel, at least one of which is an E1 intrusion. A subsequent E1 borehole changes the panel's condition to E1E2, as does an E2 borehole into a panel that has an earlier E1 intrusion. Once E1E2 conditions exist in a panel, they persist throughout the regulatory period. However, releases from a panel with E1E2 conditions are restarted for each subsequent E1 intrusion into that panel, since additional E1 intrusions may introduce new volumes of brine to the panel.

Releases to the Culebra are summed across all release pathways to the Culebra to obtain total releases to the Culebra $r_k(t)$ for the kth radionuclide at each time t. Releases to the Culebra include both dissolved radionuclides and radionuclides sorbed to colloids. The WIPP PA assumes that radionuclides sorbed to humic colloids disassociate and transport as do dissolved radionuclides; other colloid species do not transport in the Culebra (see Attachment SOTERM). The release to the Culebra is partitioned into dissolved and colloid species by multiplying $r_k(t)$ by radionuclide-specific factors for the fraction dissolved and the fraction on colloids (see Table 4.3.1). Dissolved radionuclides are transported through the Culebra.

Radionuclide transport through the Culebra is computed by the code SECOTP2D (Section PA-4.9) for partially-mined and fully-mined conditions (Section 6.4.6.2.3) as indicated in Table PA-25. These computations assume a 1 kg source of each radionuclide placed in the Culebra between 0 and 50 years, and result in the fraction of each source $f_{m,k}(t)$, where m is the mining condition and k is the index for the radionuclide) reaching the LWB at each subsequent time t. For convenience, the time-ordering of the data from SECOTP2D is reversed so that the fraction $f_{m,k}(t)$ associated with year t = 200, for example, represents the release at the boundary at year 10,000 for a release occurring between 150 and 200 years.

The total release through the Culebra $R_{Cul,k}$ is calculated for the kth radionuclide by

$$R_{Cul,k} = \sum_{t_i \le t_m} r_k(t_i) f_{PM,k}(t_i) + \sum_{t_i > t_m} r_k(t_i) f_{FM,k}(t_i), \qquad (274)$$

where $r_k(t_i)$ is the release of the kth radionuclide to the Culebra in kg at time t_i and $f_{PM,k}(t_i)$ and $f_{FM,k}(t_i)$ are the fractions of a unit source placed in the Culebra in the interval (t_{i-1}, t_i) that reaches the LWB by the end of the 10,000-year regulatory period, for partial mined and fully mined conditions within the LWB, respectively. The function $f_{m,k}(t)$ changes when mining is assumed to occur within the LWB; hence the sum in the equation above is evaluated in two parts, where t_{min} is the time that mining occurs. The total releases through the Culebra $f_{ST}(\mathbf{x}_{st})$ is computed by converting the release of each radionuclide $R_{Cul,k}$ from kg to EPA units, then summing over all radionuclides.

PA-6.8.8 CCDF Construction

For each vector $\mathbf{x}_{su,k}$ in the space of subjective uncertainty, the code CCDFGF samples a sequence $\mathbf{x}_{st,i}$, i = 1, 2, …, nS of futures. In the CRA-2004 PA, nS = 10,000; this number of futures is sufficient to generate an adequate estimate of the mean CCDF for total releases for comparison with the boundary line specified in 40 CFR § 191.13, as demonstrated in Section PA-9.1. A release $f(\mathbf{x}_{st,i})$ for each future is then constructed as described in Sections PA-6.8.1 through PA-6.8.7. Once the $f(\mathbf{x}_{st,i})$ are evaluated, the CCDF can be approximated as indicated in Equation (275).

$$prob(Rel > R) = \int_{S_{st}} \delta_R\left[f(\mathbf{x}_{st})\right] d_{st}(\mathbf{x}_{st})\, dV_{st} \cong \sum_{i=1}^{nS} \delta_R\left[f(\mathbf{x}_{st,i})\right] / nS \qquad (275)$$

A binning technique is used to construct the desired CCDF (i.e., the consequence axis is divided into a sequence of bins and the number of values for $f(\mathbf{x}_{st,i})$ falling in each bin is

accumulated). In addition, all values for $f\left(\mathbf{x}_{st,i}\right)$ are saved and subsequently ordered to provide an alternative method for constructing the CCDFs. In addition to the total CCDF for all releases, it will be possible to obtain CCDFs for individual release modes (e.g., cuttings, spallings, direct brine releases, to Culebra, through MBs, through Culebra). The logic for the production of the CCDFs is diagrammed in Figure PA-34.

The CCDF construction indicated in this section is for a single sample element $\mathbf{x}_{su,k}$ of the form indicated in conjunction with Equation (260). Repeated generation of CCDFs for individual sample elements $\mathbf{x}_{su,k}$, i.e. for the vectors representing epistemic uncertainty in the model results, will lead to the distribution of complete CCDFs.

PA-6.9 Sensitivity Analysis

Evaluation of one or more of the models discussed in Chapter PA-4.0 with the LHS in Equation (260) creates a mapping

$$\left\{x_{su,k}, y_{su,k}\right\},\ k = 1, 2, \ldots, nLHS \qquad (276)$$

from analysis inputs (i.e., $x_{su,k}$) to analysis results (i.e., $y\left(x_{su,k}\right)$), where $y_{su,k}$ denotes the results obtained with the model or models under consideration. A vector notation is used for y because, in general, a large number of predicted results are produced by each of the models used in the CRA-2004 PA. In addition, $y\left(x_{su,k}\right)$ could also correspond to a CCDF for normalized release constructed from model results associated with $x_{su,k}$. Sensitivity analysis explores the mapping in Equation (276) to determine how the uncertainty in individual elements of x_{su} affects the uncertainty in individual elements of $y\left(x_{su}\right)$. Understanding how uncertainty in analysis inputs affects analysis results aids in understanding the current PA, and aids in improving the models for future PAs.

The presentation of results from each major model in the WIPP PA is accompanied by sensitivity analyses of the most important output of each major model. Where practical, sensitivity analysis results are based on a pooling of the results obtained for the three replicated LHSs (i.e., R1, R2, R3) discussed in Section PA-6.4. In other cases, the sensitivity analysis is based on the results for the first replicate (i.e., R1), and statistics are compared across the three replicates.

Three principle techniques are used in the sensitivity analysis: scatterplots; regression analyses to determine standardized regression coefficients and partial correlation coefficients; and stepwise regression analyses. Each technique is briefly discussed. A discussion of sensitivity analyses conducted for the CCA PA is provided in Helton et al. (1998).

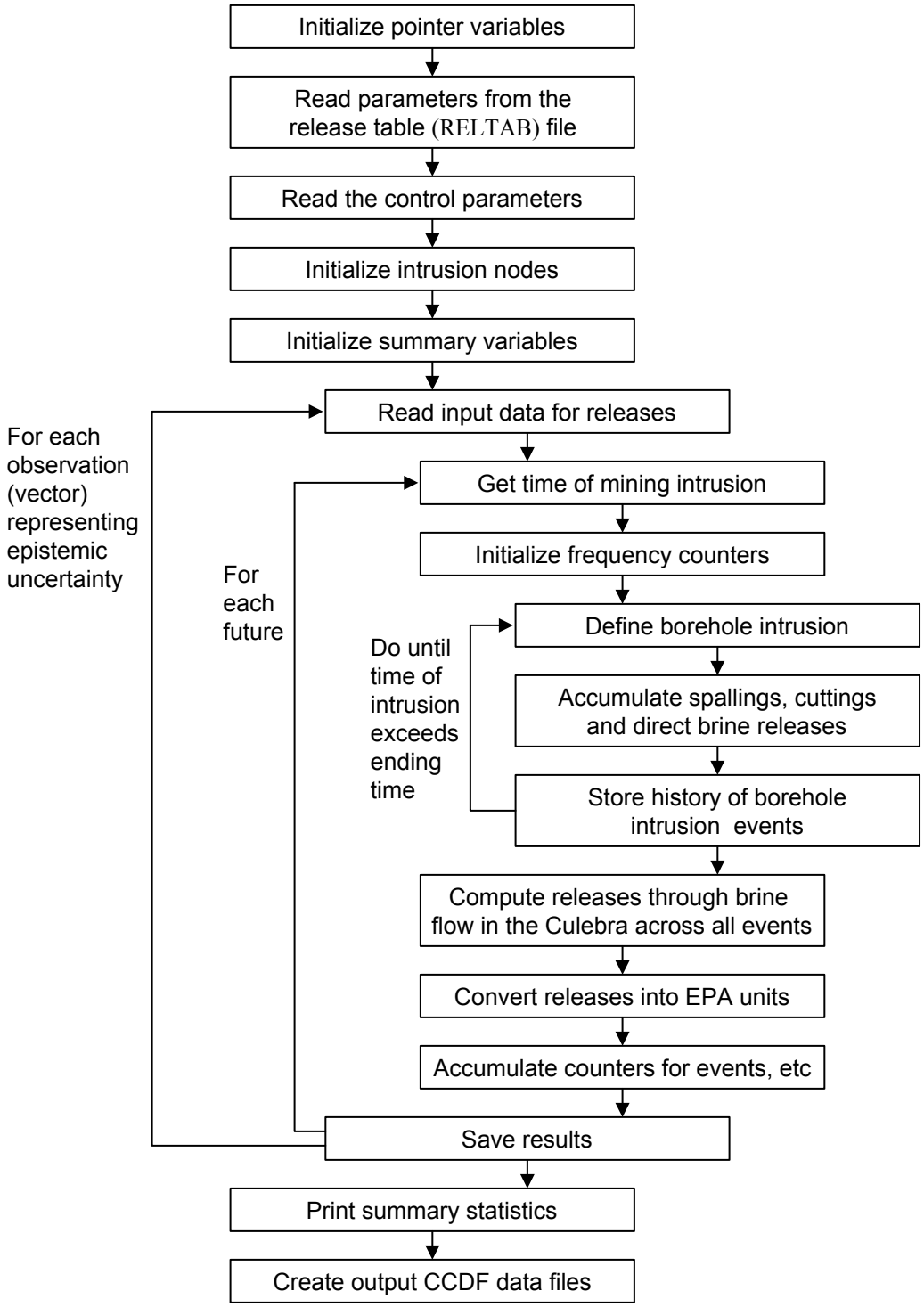

Figure PA-34. Processing of Input Data to Produce CCDFs.

PA-6.9.1 Scatterplots

Scatterplots are the simplest sensitivity analysis technique, performed by plotting the points

$$\left(x_{kj}, y_k\right),\ k = 1, 2, \ldots, nLHS \qquad (277)$$

for each element x_j of x. The resulting plots can reveal relationships between y and the elements of x (i.e., the x_j). Scatterplots can be effective at revealing nonlinear relationships or threshold values, and at screening the elements of x for further investigation. The examination of such plots when Latin hypercube sampling is used can be particularly revealing due to the full stratification over the range of each input variable. Iman and Helton (1988) provide an example where the examination of scatterplots revealed a rather complex pattern of variable interactions.

PA-6.9.2 Regression Analysis

A more formal investigation of the mapping in Equation (276) can be based on regression analysis. In this approach, a model of the form

$$y = b_0 + \sum_{j=1}^{n} b_j x_j \qquad (278)$$

is developed from the mapping between analysis inputs and analysis results shown in Equation (276), where the x_j are the input variables under consideration and the b_j are coefficients that must be determined. The coefficients b_j and other aspects of the construction of the regression model in Equation (278) can be used to indicate the importance of the individual variables x_j with respect to the uncertainty in y. The CRA-2004 PA employs the method of least squares to determine the coefficients b_j (Myers 1986).

Often the regression in Equation (278) is performed after the input and output variables are normalized to mean zero and standard deviation one. The resulting coefficients b_j are called standardized regression coefficients (SRCs). When the x_j are independent, the absolute value of the SRCs can be used to provide a measure of variable importance. Specifically, the coefficients provide a measure of importance based on the effect of moving each variable away from its expected value by a fixed fraction of its standard deviation while retaining all other variables at their expected values.

Partial correlation coefficients (PCCs) can also provide a measure of the linear relationships between the output variable y and the individual input variables. The PCC between y and an individual variable x_p is obtained from the use of a sequence of regression models. First, the following two regression models are constructed:

$$\hat{y} = b_0 + \sum_{\substack{j=1 \\ j \neq p}}^{n} b_j x_j \text{ and } \hat{x}_p = c_0 + \sum_{\substack{j=1 \\ j \neq p}}^{n} c_j x_j \ , \qquad (279)$$

Then, the results of the two preceding regressions are used to define the new variables $y - \hat{y}$ and $x_p - \hat{x}_p$. By definition, the PCC between y and x_p is the correlation coefficient between $y - \hat{y}$ and $x_p - \hat{x}_p$. Thus, the PCC provides a measure of the linear relationship between y and x_p with the linear effects of the other variables removed.

Regression and correlation analyses often perform poorly when the relationships between the input and output variables are nonlinear. This is not surprising since such analyses are based on the assumption of linear relationships between variables. The problems associated with poor linear fits to nonlinear data can be avoided by use of the rank transformation (Iman and Conover 1979). The rank transformation is a simple concept: data are replaced with their corresponding ranks and then the usual regression and correlation procedures are performed on these ranks. Specifically, the smallest value of each variable is assigned the rank 1, the next largest value is assigned the rank 2, and so on up to the largest value, which is assigned the rank m, where m denotes the number of observations. The analysis is then performed with these ranks being used as the values for the input and output variables. A formal development of PCCs and the relationships between PCCs and SRCs is provided by Iman et al. (1985).

PA-6.9.3 Stepwise Regression Analysis

Stepwise regression analysis provides an alternative to constructing a regression model containing all the input variables. With this approach, a sequence of regression models is constructed. The first regression model contains the single input variable that has the largest impact on the uncertainty in the output variable (i.e., the input variable that has the largest correlation with the output variable y). The second regression model contains the two input variables that have the largest impact on the output variable: the input variable from the first step plus whichever of the remaining variables has the largest impact on the uncertainty not accounted for by the first variable (i.e., the input variable that has the largest correlation with the uncertainty in y that cannot be accounted for by the first variable). Additional models in the sequence are defined in the same manner until a point is reached at which further models are unable to meaningfully increase the amount of the uncertainty in the output variable that can be accounted for.

Stepwise regression analysis can provide insights on the importance of the individual variables. First, the order in which the variables are selected in the stepwise procedure provides an indication of their importance, with the most important variable being selected first, the next most important variable being selected second, and so on. Second, the R^2 values at successive steps of the analysis also provide a measure of variable importance by indicating how much of the uncertainty in the dependent variable can be accounted for by all variables selected through each step. When the input variables are uncorrelated, the differences in the R^2 values for the regression models constructed at successive steps equals the fraction of the total uncertainty in the output variable that can be accounted for by the individual input

variables being added at each step. Third, the absolute values of the SRCs in the individual regression models provide an indication of variable importance. Further, the sign of an SRC indicates whether the input and output variable tend to increase and decrease together (a positive coefficient) or tend to move in opposite directions (a negative coefficient).

PA-7.0 RESULTS FOR THE UNDISTURBED REPOSITORY

The PA tabulates releases from the repository for undisturbed conditions. Releases to the accessible environment from the undisturbed repository fall under two sets of protection requirements. The first, as set forth 40 CFR § 191.15, protects individuals from radiological exposure; the second, in 40 CFR Part 191, Subpart C, protects groundwater resources from contamination. Chapter 8 describes how WIPP complies with these two requirements. This section supplements Chapter 8 by presenting flow (BRAGFLO) and transport (NUTS) results from modeling the undisturbed repository.

PA-7.1 Salado Flow

Flow in the Salado is computed by BRAGFLO (see Section PA-4.2). This section summarizes the Salado flow calculation results for the undisturbed scenario (S1). Pressure in the repository, brine saturation in the waste, and brine flow out of the repository are presented, along with sensitivity analyses that identify the uncertain parameters to which these results are most sensitive. The analysis package for Salado Flow (Stein and Zelinski 2003b) contains a detailed presentation on the BRAGFLO model, calculation results, and further sensitivity analyses.

PA-7.1.1 Pressure in the Repository

In undisturbed conditions, pressure strongly influences the extent to which contaminated brine might migrate from the repository to the accessible environment. In addition, pressure developed under undisturbed conditions is an initial condition for the models for spallings and DBR (Section PA-4.6 and Section PA-4.7, respectively).

The Salado flow model represents the repository as five regions in the numerical grid: three waste-filled regions (the Waste Panel, South RoR, and North RoR in Figure PA-8) and two excavated regions with no waste (Ops and Exp in Figure PA-8), which are combined in this analysis into the single nonwaste region. Figure PA-35 shows pressure in each region for the 100 realizations in Replicate R1. Pressures within the three waste-filled areas are very similar, because gas generation occurs in each region simultaneously. The pressure in the nonwaste region tends to be lower than in the waste-filled regions due to the intervening panel closures (CONC_PCS in Figure PA-8).

During the first 1,000 years, repository pressure may increase rapidly due to several factors: rapid initial creep closure of rooms (see Attachment PORSURF); initial inflow of brine causes gas generation due to corrosion; and availability of CPR material to produce gas by microbial degradation. Pressure generally approaches a steady-state value after 1,000 years as room closure ceases, brine inflow slows (thereby reducing gas generation by corrosion), and CPR materials are consumed.

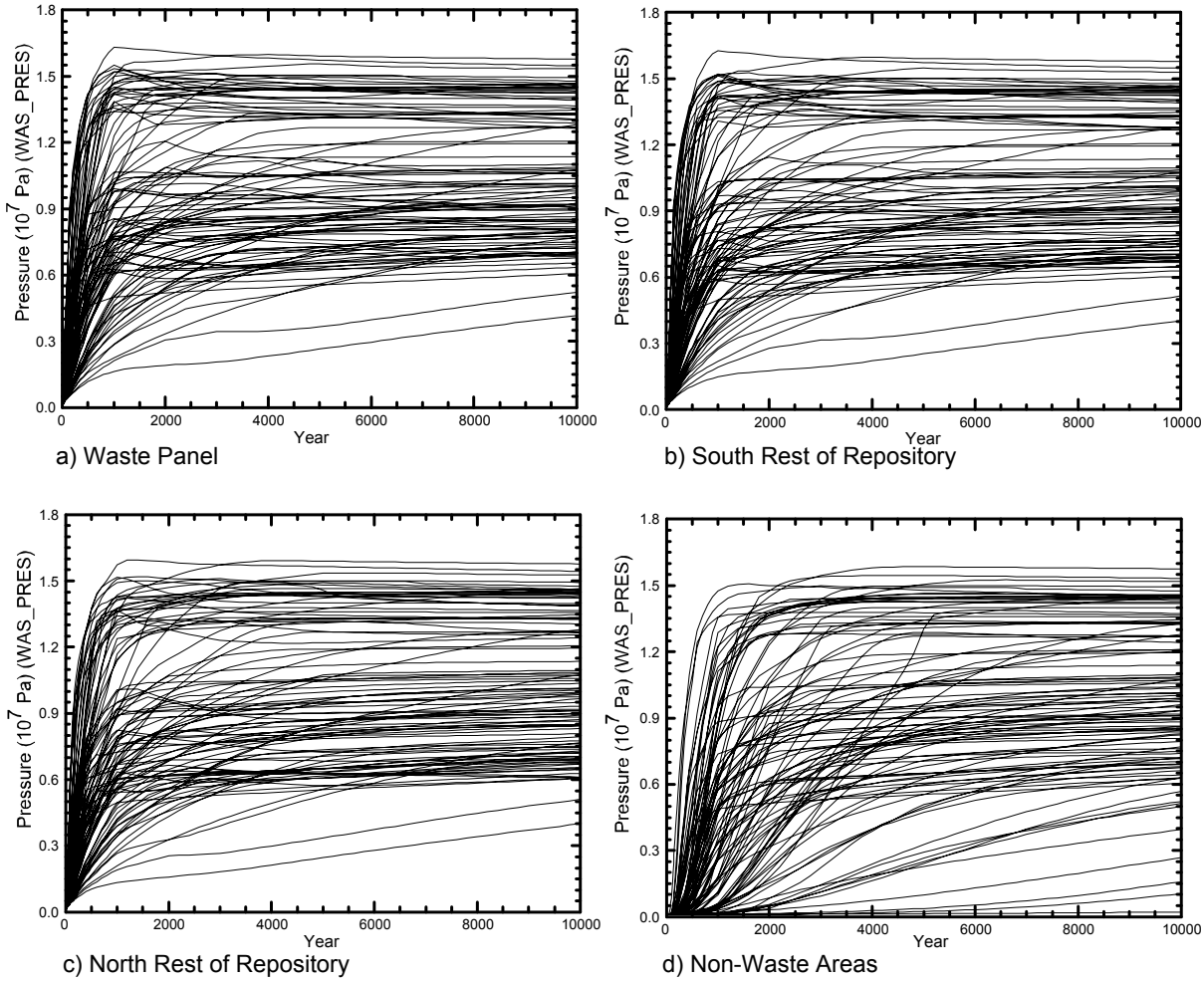

Figure PA-35. Pressure in the Excavated Areas, Replicate R1, Scenario S1.

Figure PA-36 shows the mean and 90th percentile values for pressure in each region. There is a consistent pattern of declining pressure from the waste panel through South RoR (SRR_PRES) and North RoR (NRR_PRES) to the nonwaste region (NWA_PRES). The differences in pressure reflect the slow migration of gas from waste-filled regions to the nonwaste regions where no gas is being produced. The 90th percentile pressures level off between 14 and 15 MPa indicating equilibrium between gas generation, which increases pressure, and pressure relief processes (e.g., fracturing, outward migration of fluids, and increased porosity of the excavated areas).

Sensitivity analyses are used to determine the importance of parameter uncertainty to the uncertainty in model results. Figure PA-37 shows partial rank correlation coefficients (PRCCs) resulting from regression between pressure in the waste panel (WAS_PRES) and the uncertain variables in the LHS (Section PA-5.0). The figure shows that uncertainty in the pressure in the waste panel is primarily determined by the sampled input parameter, WMICDFLG, which indicates whether microbial gas generation is active and what materials,

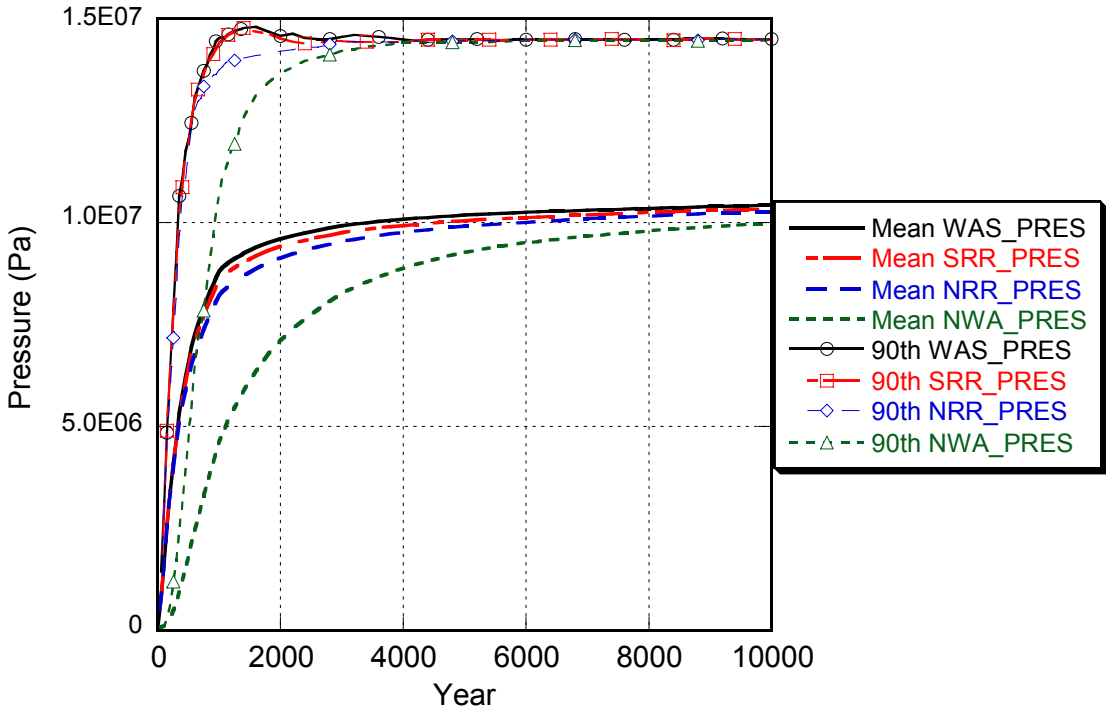

Figure PA-36. Mean and 90th Percentile Values for Pressure in Excavated Areas, Replicate R1, Scenario S1.

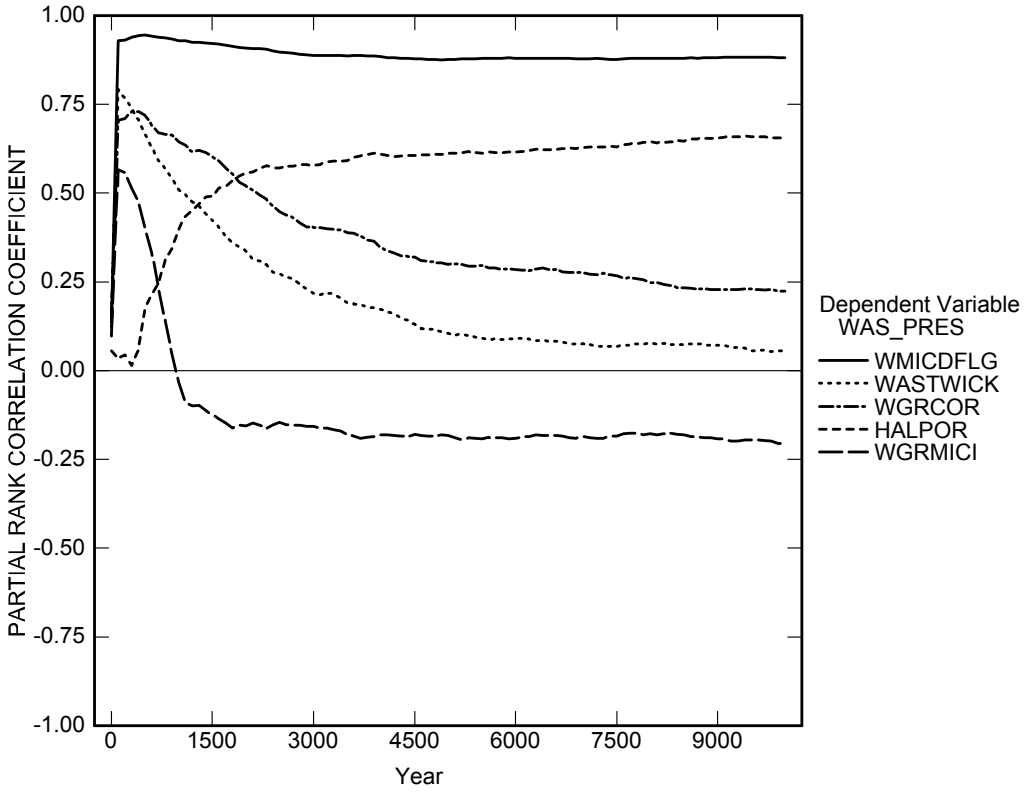

Figure PA-37. Primary Correlations of Pressure in the Waste Panel with Uncertain Parameters, Replicate R1, Scenario S1.

if any, are consumed. The positive correlation indicates that higher pressures result from higher values of WMICDFLG, which represent larger amounts of material available for gas production by microbial activity. The PRCC for WMICDFLG is approximately 0.85 throughout the 10,000-year calculation time, indicating that uncertainty in this parameter explains the variability in the waste panel pressure. Consequently, uncertainties in other parameters are not very significant; the other PRCCs in Figure PA-37 indicate that halite porosity (HALPOR), the inundated microbial gas generation rate (WGRMICI), the corrosion rate for steel (WGRCOR), and the waste wicking parameter (WASTWICK) determine the remaining variability in waste panel pressure.

Figure PA-38 compares statistics for pressure in the waste panel among the three replicates and shows that results for the three replicates are very similar. Mean pressures are nearly coincident; small differences between replicates are observable among the replicates at very high or very low pressures.

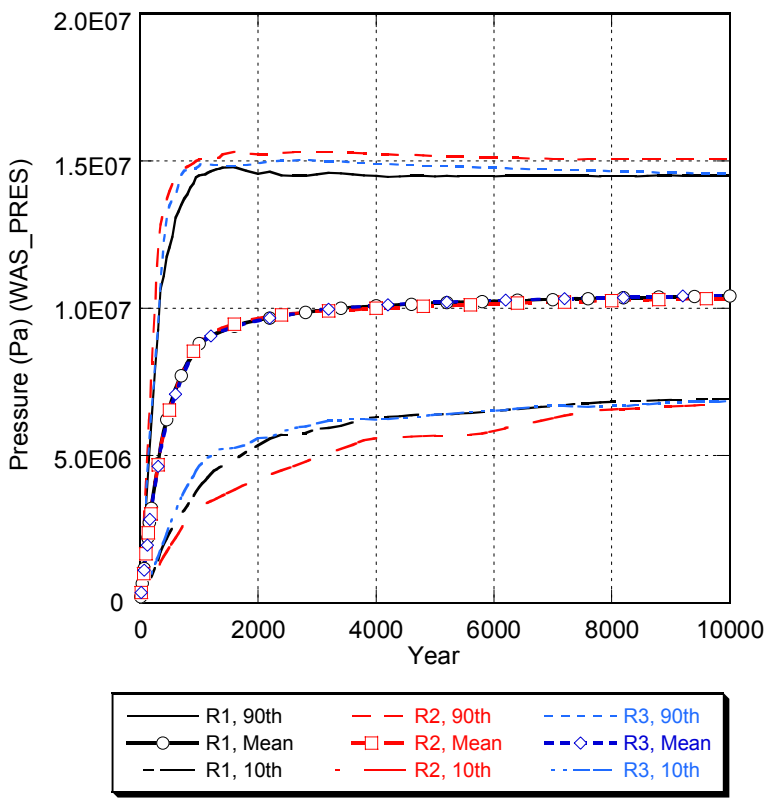

Figure PA-38. Comparison of Pressure in the Waste Panel Between All Replicates, Scenario S1.

PA-7.1.2 Brine Saturation in the Waste

Brine saturation is an important result of the model for Salado Flow, because gas generation processes, which tend to increase pressure, require brine. Brine saturation is also an initial condition in the model for DBR (Section PA-4.7).

Figure PA-39 shows brine saturation in the various excavated areas of the repository for the 100 realizations of Replicate 1. Brine saturation in the waste-filled areas is set initially to 0.015. Saturation increases very rapidly (in the first 100 years) in all excavated areas as brine flows toward the excavations, primarily from the DRZ above the excavation. Initially there is a large pressure differential between the DRZ and the excavated regions, and the relatively high permeability of the DRZ, compared to undisturbed halite, permits the rapid influx of brine. Brine inflow slows as the pressures equalize and as brine saturation in the DRZ decreases. Brine saturation in the waste decreases over time as brine is consumed by corrosion. Brine may also be driven out of the repository by high pressure.

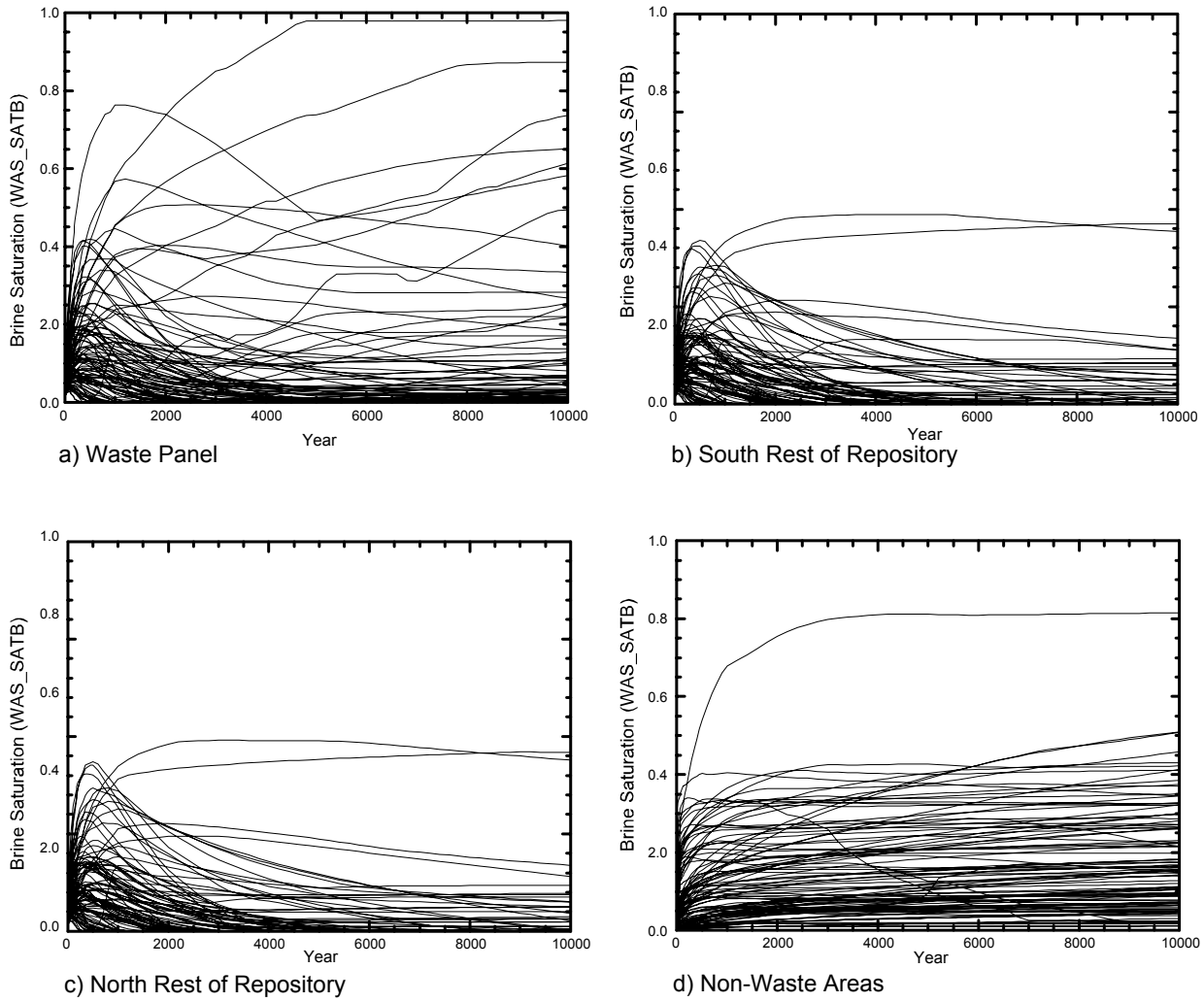

Figure PA-39. Brine Saturation in the Excavated Areas, Replicate R1, Scenario S1.

Figure PA-40 compares statistics for brine saturation between the different regions of the repository. Brine saturation in the waste panel (WAS_SATB) tends to be greater than in the rest of repository regions (SRR_SATB and NRR_SATB) due to the artificial two-dimensional modeling of the Salado; in the modeling grid (Figure PA-8), the waste panel has direct contact with the anhydrite MBs while the rest of repository regions do not. Brine saturation in the

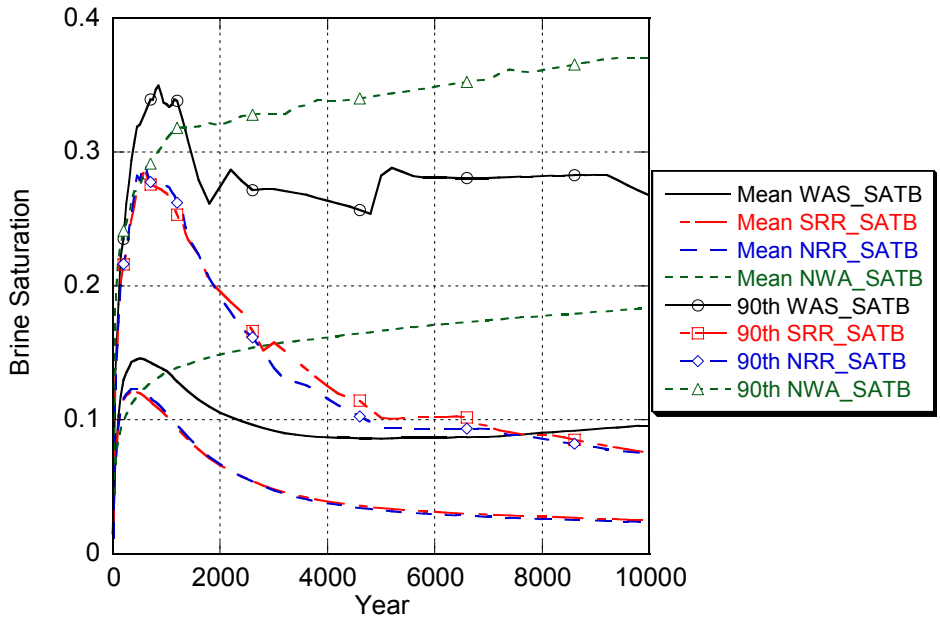

Figure PA-40. Mean and 90th Percentile Values for Brine Saturation in Excavated Areas, Replicate R1, Scenario S1.

non-waste region (NWA_SATB) is higher than in the waste-filled regions due to brine consumption in the waste regions, but also due to the panel closures. Brine that enters the experimental area flows down the stratigraphic gradient into the operations area, then ponds up against the panel closure separating the operations area from the waste filled regions.

Regression between the brine saturation in the waste panel (WAS_SATB) and the uncertain parameters in the LHS identifies a number of parameters that contribute to the uncertainty in brine saturation. The relative importance of these parameters varies over the 10,000-year modeling period, and none of the parameters is clearly dominant. Figure PA-41 shows positive correlations with halite porosity (HALPOR) and DRZ permeability (DRZPRM). Increases in halite porosity increase the volume of brine available in the material overlying the waste; increases in DRZ permeability accelerate drainage into the waste. Negative correlations are found between brine saturation and the corrosion rate (WGRCOR) and the wicking factor (WASTWICK) because increases in these two variables increase the rate at which brine is consumed by corrosion, thus decreasing saturation. The negative correlation between brine saturation and WMICDFLG, which becomes significant near the end of the simulation, indicates that increasing total gas generated (by adding microbial degradation of CPR material) eventually leads to less brine inflow and consequently lower saturation.

Figure PA-42 compares brine saturation statistics for the three replicates. The plots of the mean brine saturation are nearly coincident. Significant differences between replicates are evident at the high end of the saturation scale because there are only a few vectors in each replicate with high saturations.

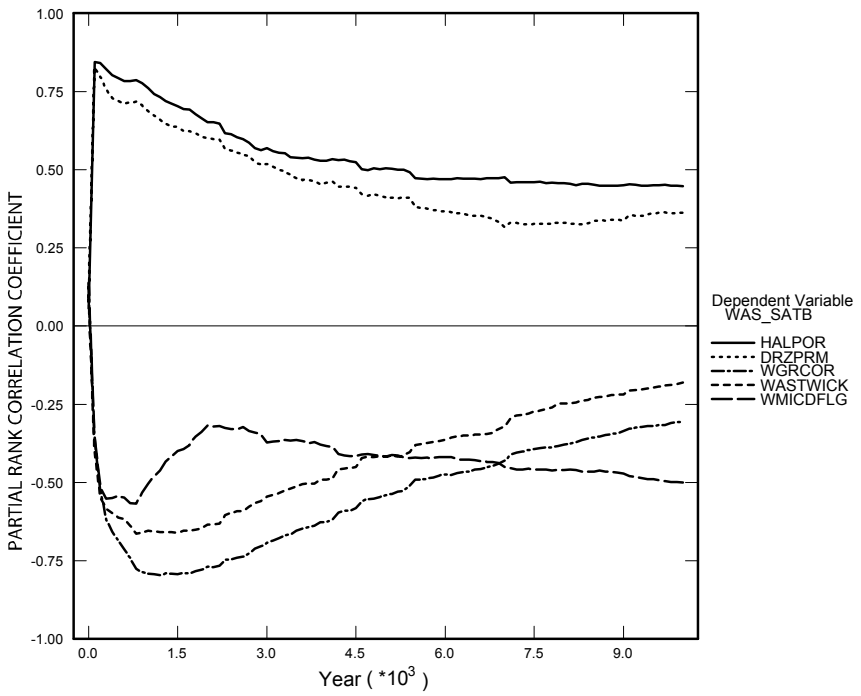

Figure PA-41. Primary Correlations of Brine Saturation in the Waste Panel with Uncertain Parameters, Replicate R1, Scenario S1.

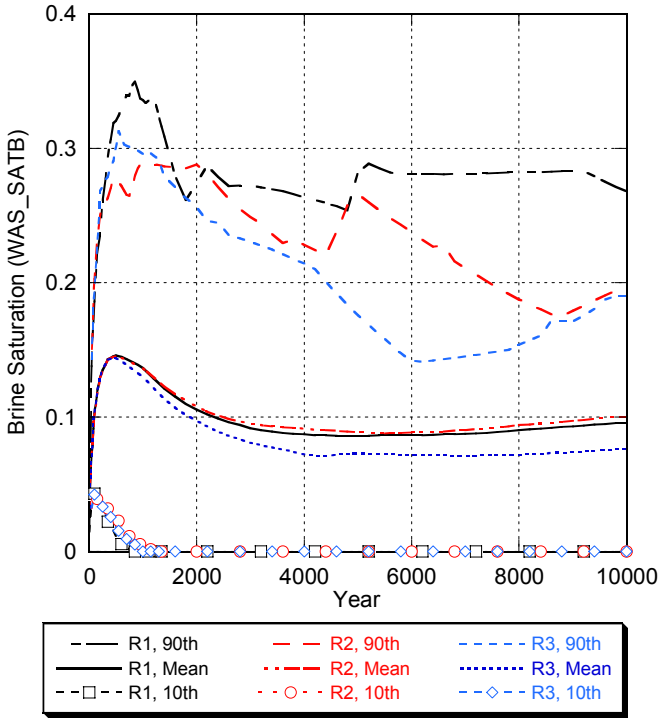

Figure PA-42. Comparison of Brine Saturation in the Waste Panel Between Replicates, Scenario S1.